



King Saud University
Arabian Journal of Chemistry

www.ksu.edu.sa
www.sciencedirect.com



ORIGINAL ARTICLE

Exploring recent advances in silver halides and graphitic carbon nitride-based photocatalyst for energy and environmental applications



Prachi Thakur^a, Pankaj Raizada^{a,b,*}, Pardeep Singh^{a,b}, Abhinandan Kumar^a,
Aftab Aslam Parwaz Khan^{c,d}, Abdullah M. Asiri^{c,d}

^a School of Chemistry, Faculty of Basic Sciences, Shoolini University, Solan, HP 173229, India

^b Himalayan Centre for Excellence in Nanotechnology, Shoolini University, Solan, HP 173229, India

^c Center of Excellence for Advanced Materials Research, King Abdulaziz University, P.O. Box 80203, Jeddah 21589, Saudi Arabia

^d Chemistry Department, Faculty of Science, King Abdulaziz University, P.O. Box 80203, Jeddah 21589, Saudi Arabia

Received 4 February 2020; accepted 20 April 2020

Available online 30 April 2020

KEYWORDS

Semiconductor-based photocatalysis;
Metal free graphitic carbon nitride (g-C₃N₄);
Localized surface plasmon resonance (LSPR);

Abstract Engineering visible light active photocatalytic systems for renewable energy production and environmental remediation has always been a promising technology to counter overall energy demands and pollution challenges. As a fascinating conjugated polymer graphitic carbon nitride (g-C₃N₄) has been developed as a hotspot in the research field as a metal-free semiconducting material with the appealing band gap of 2.7 eV. Recently, g-C₃N₄ has gained tremendous interest in photocatalytic wastewater abatement as well as for hydrogen (H₂) generation, carbon dioxide (CO₂) reduction, and pollutant degradation, under exposure to visible light. Plasmonic silver halides

Abbreviations: AOT, Advanced oxidation technologies; E_g, Band gap; BET, Brunauer-Emmett-Teller; CO₂, Carbon dioxide; CDs, Carbon Dots; e⁻_{CB}, Conduction band electrons; DFT, Density functional theory; DCF, Diclofenac; EIS, Electrochemical impedance spectroscopy; e⁻, Electron; EHP, Electron-hole pair; EDX, Energy dispersive X-ray analysis FTIR, Fourier-transform infrared spectroscopy; g-C₃N₄, Graphitic carbon nitride; h⁺, Hole; H₂, Hydrogen; ^{rad}OH, Hydroxyl radicals; IBF, ibuprofen; LSPR, Localized surface plasmon resonance; MO, Methyl orange; MB, Methylene blue; NPs, Nanoparticles; NS, Nanosheets; NTP, Nitenpyram; NOF, Norfloxacin; OWS, Overall water splitting; OA, Oxalic acid; O₂, Oxygen; PL, Photoluminescence; ROS, Reactive oxygen species; RSs, Reactive species; RhB, Rhodamine B; SEM, Scanning electron microscopy; SC, Semiconductor; Ag, Silver AgBr, Silver Bromide; AgCl, Silver chloride; AgX, Silver halides; AgI, Silver Iodide; AgNO₃, Silver nitrate; ^{rad}O₂⁻, Superoxide radical; SPR, Surface plasmon resonance; TC, Tetracycline; TGA, Thermal gravimetric analysis; TiO₂, Titanium dioxide; TEM, Transmission electron microscopy; UV, Ultraviolet; UV-Vis DRS, UV-Visible diffuse reflectance spectroscopy; e⁻_{VB}, Valence band electrons; VLT, Visible-light-triggered; H₂O, Water; XRD, X-ray diffraction; XPS, X-ray photoelectron spectroscopy

* Corresponding author at: School of Chemistry, Faculty of Basic Sciences, Shoolini University, Solan, HP 173229, India.

E-mail address: pankajchem1@gmail.com (P. Raizada).

Peer review under responsibility of King Saud University.



Pollutant mineralization;
Energy applications;
Wastewater treatment

(AgX) such as AgCl, AgBr, and AgI as plasmonic photocatalyst have received immense research interest owing to their escalating photocatalytic efficacy and strong surface plasmon resonance effect (SPR). AgX is the photosensitive, broad bandgap semiconducting materials with effectual antimicrobial properties. This review summarizes the heterostructure of carbonaceous g-C₃N₄ with plasmonic AgX, to reduce the recombination of photo-generated charge carriers, thus enhancing the natural light absorption. g-C₃N₄ grafted AgX nanoarchitectures can be utilized for several potential applications, for instance, overall water splitting (OWS), CO₂ conversion to hydrocarbon fuels, pollutant exclusion, and antibacterial disinfection. This review focuses on the evolution of g-C₃N₄ as well as AgX, facile, and synthetic routes for fabrication of g-C₃N₄ tailored AgX, construction of nano-junctions (AgX/g-C₃N₄) with various photocatalytic applications. Finally, we provided a viewpoint of current hassles and some perceptions of novel trends in this exciting as well as developing research arena.

© 2020 The Authors. Published by Elsevier B.V. on behalf of King Saud University. This is an open access article under the CC BY-NC-ND license (<http://creativecommons.org/licenses/by-nc-nd/4.0/>).

1. Introduction

Global environmental pollution poses a severe hazard to the sustainable growth of the human community. Industrial development, economic expansion, and urbanization has turned into a big challenge (Bora and Mewada, 2017; Pawar et al. 2017). Lack of access to innocuous, reliable resources of water remains a critical hurdle worldwide, causing vector-borne syndromes alike cholera, jaundice, diarrhoea, etc. The release of agricultural run-off and organic pollutants such as antibiotics, chlorinated products, etc. decreases the oxygen level for aquatic systems (Banerjee et al., 2014). According to a report of The Times of India, ministry of urban development (2013), census (2011), as well as Central Pollution Control Board, determined that 75–80% of water effluence is due to household trash, although untreated effluent flowing into water bodies have increased in later years. Every day, 2 million tons of sewage, industrial as well as agricultural scrap is dispensed into the world's water (UNWWAP 2003). As reported, about 80% of India's surface water is contaminated, as evaluated by Water Aid, an international organization working for water sanitation and hygiene. Also, Environmental Protection Agency (EPA) sets legal limits on over 90 contaminants in drinking water. The legal limit for a contaminant reflects the level that protects human health and superior water systems can be achieved using the best available technology. Indeed, conservative approaches such as coagulation, flocculation, sedimentation, reverse osmosis, filtration, adsorption, boiling, etc. were adopted for wastewater refining (Singh et al., 2017, 2019a). These conventional methods were inherited with certain downsides, i.e., these are time-consuming, induces sludge formation, give rise to secondary pollutants, applicable at small scale and consume an intensive amount of energy. This calls for the development of innovative and greener water decontamination approaches, which are economical, sturdy, and energy efficient (Mamba and Mishra, 2016; Raizada et al., 2017a). Lately, advanced oxidation technologies (AOT's) have been developed as effective filtration techniques for simulated water comprising of organic as well as inorganic toxins (Miklos et al., 2018; Pare et al., 2009). Reactive oxygen or free radicals are potent oxidants that establish AOTs to degenerate organic contaminants to reliable molecules, for instance, carbon dioxide (CO₂) and water (H₂O). Hydroxyl radicals ([•]OH) are highly reactive, owns non-selective nature, and possess compelling

oxidizing efficacy ($E^0 = +2.80$ V), and these species attack organic molecules with a rate of 10^6 – 10^9 M⁻¹ s⁻¹ (Miao et al., 2017b). [•]OH radicals rapidly disperse from the reaction solution, as a result of their short life span (ns) in water. AOTs can be categorized as homogenous and heterogeneous processes based on the phase of utilized catalyst. However, significant hindrances limiting their practical applications were a necessity of advanced paraphernalia, UV light absorption, high energy demands, partial decomposition of noxious waste as well as expensiveness of these techniques (Raizada et al., 2017b; Akhundi and Habibi-Yangjeh, 2016b; Sharma et al., 2019). To resolve these hitches, photocatalytic systems have fascinated enormous research interest as it offers greener and productive routes for various ecological issues (Raizada et al., 2020a; Shandilya et al., 2020). Among most of the alternatives, semiconductor mediated photocatalysts have appeared as the most enticing and propitious technologies employing natural energy for environmental restoration. In the year 1972, Fujishima and Honda introduced semiconductor photocatalysis for overall water splitting (OWS) to hydrogen (H₂) production using a metal oxide, especially titanium dioxide (TiO₂) (Fujishima and Honda, 1972). TiO₂ has been widely employed for oxidative decay of pollutants due to its high abundance, inexpensiveness, non-toxic nature, insolubility in water, and high chemical inertness. However, lower absorption of visible light and less quantum yield may be accredited to a wide bandgap, i.e., 3.2 eV, which confines its applications in the visible range (Lai et al., 2016). The progressions in high-performance visible light-triggered (VLT) photocatalysts are more compelling due to pronounced visible light in the solar spectrum (43%) as compared with typically used photocatalytic materials, which absorb merely ultraviolet (UV) light (4% of solar spectrum). After that, heterogeneous photocatalysis has been enormously employed in water splitting to H₂ and O₂ (Mousavi and Habibi-Yangjeh, 2017; Appavu et al., 2016; Yamasita et al., 2004), water/air cleansing (Raizada et al., 2016; Singh et al., 2014; Fujishima et al., 2000), CO₂ reduction (Wang et al., 2015; Liu et al., 2018), self-cleaning (Zhang et al., 2005; Malato et al., 2009), selective organic alterations (Lang et al., 2014) and high-efficiency solar cells (O'regan and Grätzel, 1991). Owing to properties such as; (i) complete mineralization of pollutants without the formation of any secondary product, (ii) economical, and (iii) viable operational temperature as well as pressure has prolonged the

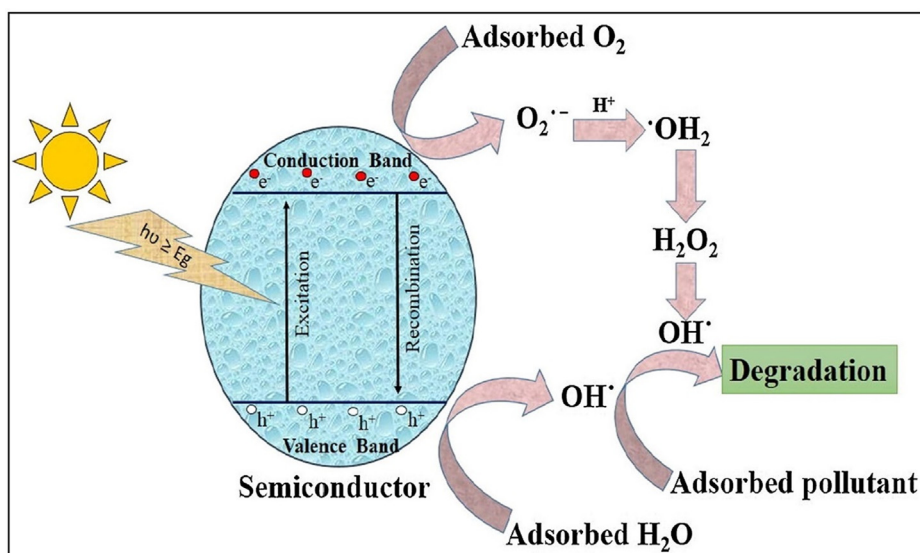


Fig. 1 General photocatalytic mechanism of a photocatalyst explicating mineralization of organic pollutant; reprinted under licence from CC BY-NC-ND 4.0 (Singh et al., 2020).

implementations of heterogeneous photocatalysis in wastewater treatment (Chong et al., 2010).

Fig. 1 (Singh et al., 2020) explicated the basic photocatalytic process, where semiconducting material upon illumination to UV light with equivalent or more than the bandgap energy (E_g) gets excited resulting in the generation of electrons (e^-) and holes (h^+) in their respective conduction band (CB) and valence band (VB). These valence band holes (h_{VB}^+) and conduction band electrons (e_{CB}^-) result in the formation of electron-hole pairs (EHP). The oxidative holes and reductive electrons contribute to the redox process over the surface of semiconducting material, respectively, (Xue et al., 2018). For mineralization of target pollutants, h^+ could straight away oxidize contaminants or react with H_2O/OH^- to form $\cdot OH$ radicals. Also, e^- capture oxygen (O_2) to form superoxide radical ($\cdot O_2^-$), which not only hinders the spatial charge separation of photo-induced charge carriers however prolongs the lifetime of h^+ , while this generated h^+ as well as $\cdot O_2^-$ were responsible for pollutant deprivation. The generation of $\cdot O_2^-$ radical by a reaction of photo-induced e_{CB}^- with O_2 plus formation of $\cdot OH$ radicals by the reaction among h_{VB}^+ is specified by equation Eqs. (1) and (2);



Alternatively, for energy conversion, CO_2 could be photo reduced to useful fuels, whereas H_2O/OH^- could be oxidized to O_2 . The reactive oxygen species (ROS) released during the photocatalytic process were h^+ , $\cdot O_2^-$, H_2O_2 , and $\cdot OH$ by reacting with O_2 or H_2O/OH^- , facilitating the removal of organic/inorganic toxins present in water (Hasija et al., 2019b; Singh et al., 2020; Raizada et al., 2019c). ROS exhibits strong oxidizing ability, therefore increases reaction kinetics and effectively degrade the evolving pollutant (Zheng et al., 2017; Raizada et al., 2014; Gautam et al., 2017). Notably, not all photo-illuminated e^- take part in surface reactions, but some of the photocarriers recombine with h_{VB}^+ ensuing depressed

photocatalytic ability. Hence, to boost the photocatalytic efficiency recombination rate of photo-charge carriers must be suppressed, promoting their transference to semiconductor surface where e^- and h^+ reacted with O_2 and H_2O to generate $\cdot O_2^-$ along with $\cdot OH$, correspondingly. The reported literature revealed the exclusion of metal ions as well as inorganic ions by photocatalytic methods (Mousavi and Habibi-Yangjeh, 2018a). Several metal oxide semiconducting materials such as CaO , $BiTiO_3$, $ZnWO_4$, Fe_2O_3 , WO_3 , Nb_2O_5 , $BiOCl$, $EuVO_4$, $SrTiO_3$, ZrO_2 , Ag_2CO_3 , Bi_2WO_6 , $BiOI$, Ag_3PO_4 , $CaFe_2O_4$, $MnFe_2O_4$, $ZnFe_2O_4$, CdS , AgI , $SmVO_4$, $MnFe_2O_4$, $BiVO_4$, $g-C_3N_4$, $BiOBr$, etc. have been utilized as photocatalysts for deterioration and is endlessly growing day by day (Sudhaik et al., 2018a; Yi et al., 2019; Raizada et al., 2019c; Zhang et al., 2017b; Zhang et al., 2009a). However, their wide bandgap, rapid recombination of photo-induced EHP, lower visible light absorption, and photo deterioration remains the obstacles of semiconductor photocatalysis for pollutant degradation and several other practical implementations (Raizada et al., 2017c; Shandilya et al., 2019; Hua et al., 2019; Singh et al., 2019b). Since past years, photocatalysis has been established as an efficient approach for OWS, CO_2 conversion to energy fuels and wastewater treatment by photodegrading microbes, pharmacological leftover, antibiotics, dyes as well as phenols (Shandilya et al., 2018b; Priya et al., 2016; Patial et al., 2020). Ameliorated photocatalytic efficiency can be obtained by:

- (i) surface functionalization via integration of co-catalyst,
- (ii) surface modulation by molecular as well as elemental doping, and
- (iii) construction of typical and Z-scheme based nano-heterojunctions.

Out of the above-mentioned strategies coupling of more than two semiconductors with appropriate band, gaps have achieved massive interest owing to (i) natural light absorption of a wide-ranging bandgap semiconductor can be enhanced by

hybridizing with narrow bandgap semiconducting material, (ii) persuaded electric field excites the transference and segregation of photo-generated charge carriers, and (iii) in different semiconducting photocatalyst e^- and h^+ possessing greater redox as well as oxidative potentials simultaneously, enhances the redox capability (Chandel et al., 2020; Gautam et al., 2016; Shandilya et al., 2018a; Singh et al., 2019c).

In previous years, carbon-based materials showed tremendous ability to increase the photocatalytic activity of semiconducting materials. Carbon-based photocatalyst, for example, carbon nanotubes (CNTs), graphene, graphene oxide (GO), fullerene (C_{60}), carbon quantum dots (CQDs), carbon fibers (CF), activated carbon (AC) and carbon black behaves as photosensitizers, act as co-catalyst and possesses large specific surface area for adsorption due to their active sites. Carbon materials have a band gap narrowing effect and act as supporting material. These carbon-based materials enhance the structural stability of semiconducting materials and minimize the aggregation of particles (Cao and Yu, 2016).

1.1. Polymeric graphitic carbon nitride ($g-C_3N_4$) as photocatalyst

Graphitic carbon nitride ($g-C_3N_4$), a 'golden photocatalyst,' has provoked ripples of excitement in research societies due to its maximum visible light absorption, cost-effectiveness, greater profusion, non-toxicity, π -conjugated assembly and thermal as well as chemical stability. $g-C_3N_4$ spurred our enormous attention in 1834 due to its tunable bandgap of 2.7 eV with VB and CB potentials positioned at -1.09 and $+1.56$ eV, respectively. Owing to these properties, $g-C_3N_4$ acts as a favourable photocatalytic material and has wider applications in electrochemical water splitting, act as a photocatalyst for H_2 production as well as for photodegradation of noxious waste (Ong et al., 2016). Although, photocatalytic efficiency of bulk $g-C_3N_4$ is bounded due to (i) its inefficiency to absorb visible light (ii) higher photo-induced EHP recombination (iii) smaller surface area and (iv) lower electrical conductivity. Consequently, several modification approaches have been developed to accomplish spatial charge separation of photo-carriers such as; (1) deposition of metals/non-metals (doping), (2) fabricating porous structures and (3) coupling with alternative semiconductor (heterojunction) in order to boost the photoactivity of $g-C_3N_4$ (Sudhaik et al., 2018b). Hybridizing $g-C_3N_4$ with another semiconducting material is a notable technique because of its ability to achieve efficient transference/separation of photo-generated EHP and appropriate redox potential for photocatalytic implementations (Raizada et al., 2019d; Raizada et al., 2020).

1.2. Electronic structure of $g-C_3N_4$

In recent years' carbon nitrides (C_3N_4) have gained remarkable attention as a polymeric semiconducting material. The structure of carbon nitride (C_3N_4) materials consist of two-dimensional (2D) sheets of triazine (1,3,5-triazine, C_3N_3) and heptazine (1,3,4,6,7,9,9b-heptaazaphenalene, C_6N_7) core (Kroke et al., 2002). These are aromatic molecules where carbon (C) and nitrogen (N) atoms are arranged in alternative positions in the ring. C_3N_4 exists in seven stages, and these are categorized as $\alpha-C_3N_4$, $\beta-C_3N_4$, cubic C_3N_4 , pseudocubic

C_3N_4 , g-h-triazine, go-triazine and g-h-heptatriazine having bandgap potentials of 5.49, 4.85, 4.30, 4.13, 2.97, 0.93 and 2.88 eV, correspondingly (Teter and Hemley, 1996). Several allotropes of C_3N_4 can be fabricated *via* temperature assisted process such as heating melamine to $317^\circ C$ leads to the formation of melam $[(H_2N)_2(C_3N_3)_2]NH$ which on further heating forms melem (tri amino-heptazine) $C_6N_7(NH_2)_3$ (Jürgens et al., 2003). Above $520^\circ C$, melem condenses, and forms amine linked heptazine units, which is referred to as Liebig's melon (Liebig, 1844). Pyrolysis of cyanamide, dicyanamide, urea, thiourea, and other molecules comprising of C and N above $520^\circ C$ are considered as Polymeric carbon nitride (PCN) called melon (Kessler et al., 2017). The condensation of melem under $520^\circ C$ forms triazine based graphitic carbon nitride ($g-C_3N_4$). $g-C_3N_4$ exists as the most substantial allotrope of carbon nitride, while tri-s-triazine based $g-C_3N_4$ was the utmost steady stage at ambient environments and was dynamically favourable. Furthermore, density functional theory (DFT) measurements were accomplished by Kroke and his research group to explore its electronic structure. P_z orbitals of N and C were mainly liable for the construction of VB and CB, as investigated by DFT calculations (Ong et al., 2016). As per reports, lone pair of e^- on N atom was the reason for the formation of electronic structure and VB. Since 2009, $g-C_3N_4$, an n-type semiconducting material, has evolved as a prominent visible light active photocatalyst for degradation of organic toxins from aqueous phase (Kumar et al., 2019; Raizada et al., 2019a).

Fig. 2 illustrated various precursors for facile fabrication of $g-C_3N_4$ photocatalyst. Several physical as well as chemical approaches have been adopted for preparation of $g-C_3N_4$ photocatalyst. Mainly, top down and bottom up approaches have been embraced. Top down approach implicates breaking up of bigger $g-C_3N_4$ blocks into smaller units, namely $g-C_3N_4$ nanosheets, while bottom up approach involves incorporation of smaller molecules to form larger complex molecules. Moreover, thermal polymerization, solvothermal technique, sol-gel process, template assisted method and ionothermal approaches were commonly used for synthesis of $g-C_3N_4$ photocatalyst (Sudhaik et al., 2018b; Bojdys et al., 2008; Zhang et al., 2018).

1.3. Silver halides (AgX) as potential visible light assisted photocatalyst

Fabrication of photocatalyst with extended visible light absorption, plasmonic photocatalytic materials have gained enormous research interests. The plasmonic photocatalyst, mainly silver (Ag) and gold (Au), unveil greater absorption coefficients in wide UV-visible-near infrared range (NIR). This can be accredited to their strong surface plasmon resonance (SPR) (Zhang et al., 2009b; Huang et al., 2006). Particularly, Ag NPs were chosen due to their inexpensiveness as compared to Au NPs, and they exhibited efficient plasmon resonance in solar light (Awazu et al., 2008; Georgekutty et al., 2008).

A collective oscillation of e^-_{CB} exhibited by noble metal NPs leads to an oscillating electric field. While these oscillations caused a rearrangement of charge density as well as electric field, therefore generating professed localized surface plasmon (LSP) through a coulombic refurbishing potency to repel the

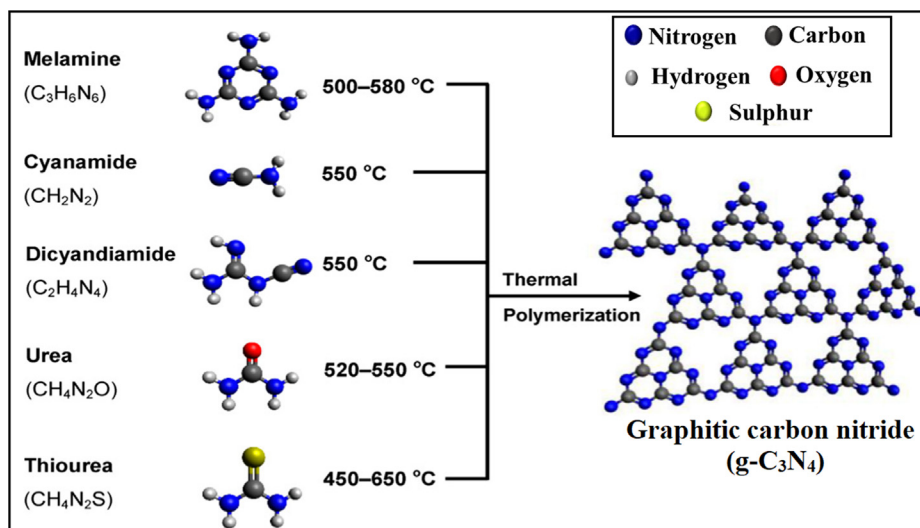


Fig. 2 Schematic representation of synthesis process of $g\text{-C}_3\text{N}_4$ by thermal polymerization of various precursors (Reproduced with permission).

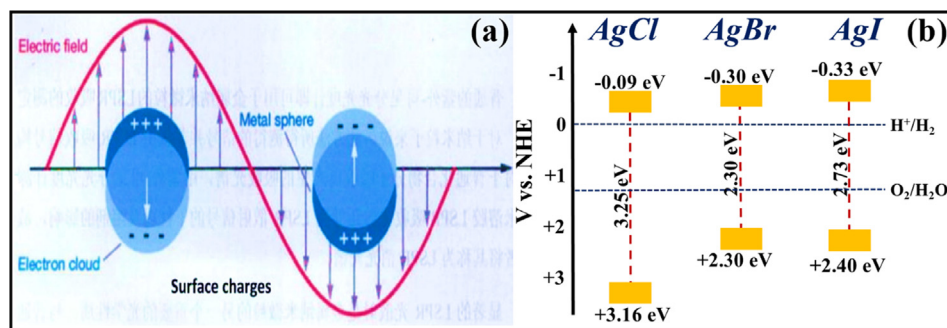
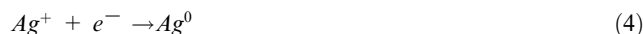
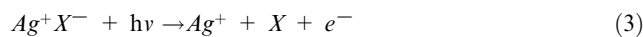


Fig. 3 Schematic illustration of (a) Surface Plasmon Resonance (SPR) in a noble metal particle; reprinted with permission from Elsevier (Licence no. 4742480664982) (Ye et al., 2012), and (b) Band gap positions of AgCl, AgBr and AgI with their respective valence band and conduction band potentials (Ye et al., 2014; Yao et al., 2016; Islam et al., 2016).

effect of positive nuclei. Plasmon resonant frequency of noble metal nano-junctions overlays the solar spectrum thereby, extending the natural light absorption. When oscillations befall at localized surface plasmon resonance (LSPR) wavelengths, i.e., 530–600 nm, the dissipated energy is assumed to be least, and consumption of natural light is maximum. Under exposure to solar light, SPR of noble metal NPs usually occurs when the frequency of stimulating light is equivalent to the rate of oscillating surface e^- (Fig. 3a) (Ye et al., 2012; Wang et al., 2012). Noble metal NPs exhibiting LSPR effect, ameliorated the efficacy of semiconductor-based photocatalysis by interacting between free surface e^- and photons, moreover tailoring novel plasmonic photocatalysts (Sarina et al., 2013; Ingram et al., 2011; Primo et al., 2011).

Till date, much attention has been gained by Ag-based photocatalysts (such as Ag_3PO_4 , AgVO_3 , Ag_2CO_3 , AgX ($X = \text{Cl}, \text{Br}, \text{I}$), Ag@AgX ($X = \text{Cl}, \text{Br}, \text{I}$), AgIO_3 , and Ag_2WO_4) for photocatalytic degradation of organic toxins. Silver halides (AgX , $X = \text{Cl}, \text{Br}, \text{I}$) being plasmonic photocatalyst with antibacterial properties are the photosensitive semiconducting materials with ameliorated visible light absorption, and their photosensitivity proposes potential utilization in photocataly-

sis. They have been broadly exerted as source materials in photographic films and employed as photosensitizers. Also, they can be used as metallic silver precursors (Archana et al., 2015). Under exposure to visible light, AgX undergoes a reduction of Ag^+ into Ag^0 , as depicted in equation Eqs. (3) and (4) (Tate, 2012);



Ag/AgX photocatalyst can be attained from AgX by exploiting their photosensitivity. These photocatalysts are highly efficacious as well as stable under visible light radiation. Despite their broad bandgap, greater than the edge of natural light, AgX has been developed as visible light assisted photocatalytic material (Grzelczak and Liz-Marzán, 2014). However, the photo-corrosive nature of Ag-based compounds limits the practical implementations of AgX as photocatalysts. Therefore, silver chloride (AgCl) having bandgap of 3.25 eV with VB and CB potentials positioned at +3.16 eV and -0.09 eV, respectively (Ye et al., 2014), while silver bromide (AgBr) has a bandgap of 2.60 eV with VB and CB potential

located at +2.30 eV and -0.30 eV, respectively (Yao et al., 2016). Also, silver iodide (AgI) possesses a band gap of 2.73 eV with VB potential at +2.40 eV and CB potential at -0.33 eV (Islam et al., 2016). Fig. 3b depicted the band gap positioning of AgCl, AgBr and AgI, respectively. Therefore, coupling of a semiconductor with another semiconducting material has emerged as a new technology for boosted photocatalytic performance (Hasiija et al., 2019a). Precisely, coupling of Ag-based photocatalysts with another semiconductor material having appropriate band edge positioning can effectively migrate and separate charge carriers which further participate in photocatalytic reactions. As a consequence, the availability of electrons which participate in the photo-reduction of Ag^+ into Ag^0 reduced significantly providing superior stability to the system (Chen et al., 2015b; Liu et al., 2011). Chen et al. tailored plasmonic Ag/AgBr/g- C_3N_4 photocatalyst via a superficial means for mineralization of methylene blue (MB) under solar light irradiation. Ag/AgBr with 40% content exhibited superior photocatalytic activity, which was about 2.4 and 1.9 times greater than bare g- C_3N_4 and Ag/AgBr hybrid. Scanning electron microscopy (SEM) analysis confirmed the deposition of sphere-like Ag/AgBr particles on aggregated g- C_3N_4 nanosheets (NS) (Fig. 4a). Moreover, particle size of Ag/AgBr particles ranging between 50 nm and 200 nm was observed in transmission electron microscopy (TEM) images. The proposed mechanism (Fig. 4b) for Ag/AgBr/g- C_3N_4 nanocomposite, suggesting the boosted photocatalytic efficacy was attributable to the synergetic effect of Ag, AgBr, and g- C_3N_4 . Under solar light illumination, both g- C_3N_4 (2.7 eV) and AgBr (2.6 eV) get excited, succeeding in the transference of photo-generated e^- from g- C_3N_4 to CB of AgBr, thereby reacting with adsorbed O_2 to produce CO_2 . Furthermore, metallic Ag produced photo-induced e^- on the AgBr surface because of a strong SPR effect. AgBr possesses inferior fermi level than that of Ag ensuing transfer of e^- from Ag to AgBr and lastly transference to adsorbed O_2 to generate O_2^- (Chen et al., 2015a, 2015b). Fig. 5(a–c) depicted facile routes for preparation of AgCl, AgBr and AgI, respectively, employing various precursors.

Recently, g- C_3N_4 grafted AgX heterojunctions have witnessed surge interest of the research community owing to its potential to minimize the recombination of photo-excited charge carriers, thereby augmenting the solar light absorption.

For example, Lan et al. delineated an integral report on highly efficient solar light assisted AgX@g- C_3N_4 (X = Cl, Br, I) photocatalyst for photodegradation of pollutants (Lan et al., 2013). In this research article, they discussed AgX and g- C_3N_4 , preparation of AgX@g- C_3N_4 nanocomposite, briefly discussed the results along with the degradation mechanism for mineralization of methyl orange (MO) dye. In another report, Xu et al. explored AgX/g- C_3N_4 (X = Br, I) nanohybrid with synergistic photocatalytic efficiency (Xu et al., 2013a). Keeping in mind the studies mentioned above, we have tried to present an extensive report on cutting-edge trends in AgX/g- C_3N_4 hybrids emphasizing pollutant mineralization accompanied by energy applications. To best of our knowledge, no review article has been published to date, as per Scopus data. Therefore, in focus of this review, we have discussed comprehensively g- C_3N_4 and AgX nanostructures, synthetic routes for facile fabrication of AgX/g- C_3N_4 nanocomposite, engineering AgX/g- C_3N_4 nano-junctions involving type-II and Z-scheme based heterostructures along with their practical implementations in photocatalytic degradation processes and energy conversion followed by bacterial disinfection. To get an overall idea of literature being reported on AgX/g- C_3N_4 composite “Scopus” database has been carried out to acquire effective outcomes. Consistent with Scopus data, we got 970, 165, 85 and 89 results employing keywords such as “g- C_3N_4 + AgCl photocatalyst”, “g- C_3N_4 + AgBr photocatalyst”, “g- C_3N_4 + AgI photocatalyst” and “g- C_3N_4 + AgX photocatalyst”, respectively, from 2009 to December 2019 (Fig. 6a–c). With such an escalating amount of reports on g- C_3N_4 tailored AgX, it is the apt and high time to impart an extensive review of AgX/g- C_3N_4 nanomaterials. Herein we presented a substantial and efficient review of this evolving hot research area.

2. Synthetic strategies for fabrication of AgX/g- C_3N_4 nanohybrids

2.1. Precipitation method

Precipitation method is often employed for AgX/g- C_3N_4 nanocomposite fabrication. Mohamed et al. explored AgCl@p-g- C_3N_4 nano photocatalyst, where mesoporous

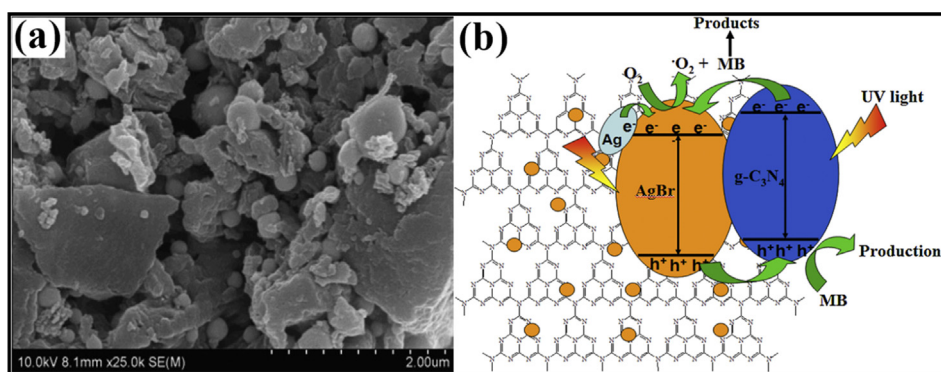


Fig. 4 (a) SEM imageries of Ag/AgBr/g- C_3N_4 nanohybrid depicting deposition of Ag/AgBr particles on aggregated g- C_3N_4 NS, and (b) Mechanistic view of Ag/AgBr/g- C_3N_4 composite explicating boosted photocatalytic efficiency; reproduced with permission from Elsevier (Licence no. 4746461343390) (Chen et al., 2015).

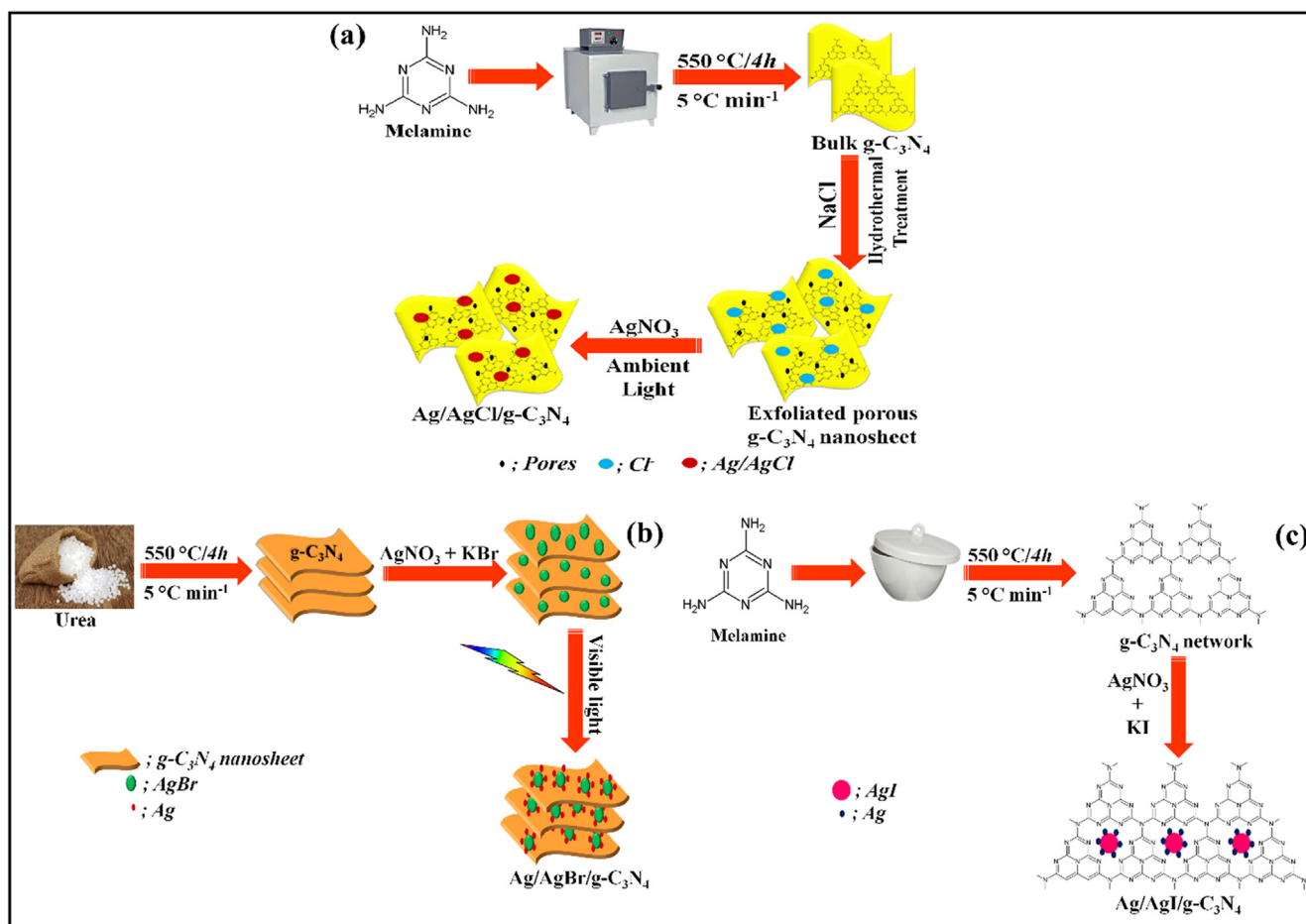


Fig. 5 Synthesis scheme for facile fabrication of (a) AgCl, (b) AgBr and (c) AgI.

graphitic carbon nitride (pg-C₃N₄) was fabricated via pyrolysis of dicyandiamide and urea at an atmospheric environment. Silver nitrate (AgNO₃) and potassium chloride (KCl) were employed as starting materials, and the AgCl@pg-C₃N₄ composite was prepared *in-situ*. The photocatalytic ability of prepared samples was estimated for photodegradation of atrazine. No peak for AgCl was observed during X-ray diffraction (XRD) analysis due to lower AgCl content or successful dispersal of AgCl onto a g-C₃N₄ surface (Fig. 7a). UV-Visible diffuse reflectance spectroscopy (UV-DRS) spectra revealed that increased weight percentage of AgCl above 3% shifted the absorption edges of pg-C₃N₄ towards extended wavelengths because higher weight percentage increases the agglomeration and size of AgCl, which reduces the absorption edge (Mohamed, 2015). Yao et al. investigated novel Ag/AgCl/g-C₃N₄ nanocomposite by precipitation in geothermal water at ambient temperature. Geothermal water is a sort of natural heat energy and renewable energy resource, which provides green energy. Here, geothermal water was employed as a chlorine source for the preparation of AgCl NPs. 50% Ag/AgCl/g-C₃N₄ revealed more excellent photocatalytic capability for the elimination of organic dyes under illumination of natural light. SEM studies explained that the deposition of Ag/AgCl NPs onto the surface of g-C₃N₄ lead to an irregular surface and a close interface was formed among g-C₃N₄ and Ag/AgCl. Also, TEM analysis illustrated the decoration of several shady Ag/

AgCl NPs on lamellar g-C₃N₄ nanosheets, with greater dispersion (Yao et al., 2014).

The advantages increasing the utilization of precipitation method for facile preparation of NPs are the relatively low reaction temperatures, fine and uniform particle size with weakly agglomerated particles, low cost and homogeneity of component distribution. Moreover, the precipitation method is not considered as a controlled process in terms of reaction kinetics. Also, the as-prepared solids have a wide particle size distribution, uncontrolled agglomerated morphology and incomplete precipitation of metal ions (Deraz, 2018).

2.2. Deposition precipitation method

A plasmonic Z-scheme based AgCl/Ag/g-C₃N₄ photocatalytic material was fabricated by Bao and his research group employing melamine (C₃H₆N₆), hexadecyl trimethyl ammonium chloride (CTAC), AgNO₃ as a precursor molecule. The photocatalytic efficiency of prepared nano-sample was explored for photodegradation of MO dye. The results revealed, Ag/AgCl NPs with a particle size of 5–15 nm were evenly distributed onto a g-C₃N₄ network. TEM studies demonstrated a lamellar sheet-like assembly and amorphous nature of pure g-C₃N₄. However, Ag/AgCl exhibits spherical morphology. It was observed that Ag/AgCl particles (dark spots) were evenly dispersed on the g-C₃N₄ surface. A slight

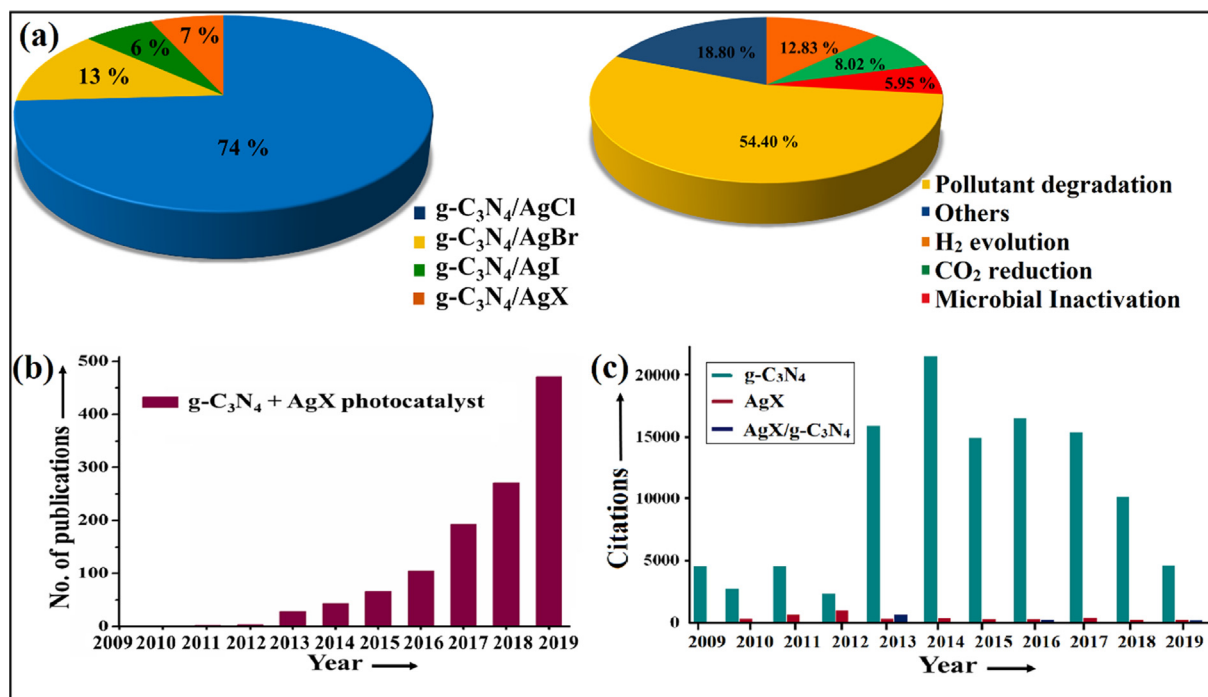


Fig. 6 Scopus data analysis (a) Pie diagram depicting multifunctional applications of AgX/g-C₃N₄ photocatalyst, (b) Bar graph portraying annual publications, and (c) Citations of g-C₃N₄, AgX as well as AgX/g-C₃N₄ photocatalyst from year 2009 to December 2019.

redshift was found in the absorption edge by UV-DRS spectra of AgCl/Ag/g-C₃N₄ composite, which may be accredited to the SPR effect of Ag crystal, i.e., formed *in-situ* on AgCl surface. Also, superior photocatalytic efficacy of AgCl/Ag/g-C₃N₄ nanocomposite was indexed to the SPR of Ag nanocrystal (Bao and Chen, 2016).

Cao and co-workers fabricated a proficient VLT Ag/AgBr/g-C₃N₄ photocatalyst using C₃H₆N₆, sodium bromide (NaBr), and AgNO₃ as predecessors for the exclusion of MO dye. The superior photocatalytic ability was observed for 50% Ag/AgBr/g-C₃N₄ nanocomposite, which may be accredited to metallic Ag and synergistic effects of AgBr/g-C₃N₄ alliance. Fig. 7b explained XRD pattern indicating face-centered cubic assembly of AgBr, where small amounts of Ag⁺ were reduced to metallic Ag, and no prominent peaks for metallic Ag were obtained. TEM imaginings (Fig. 7c) confirmed the formation of as-synthesized nanocomposite possessing random microstructure (Cao et al., 2013). Ag/AgBr tailored graphite-like carbon nitride was synthesized by Xu and his research group via deposition-precipitation method (Xu et al., 2013b). Yang et al. explored novel Z-scheme Ag@AgBr/g-C₃N₄ plasmonic photocatalyst by photoreduction of AgBr/g-C₃N₄ nanohybrid. Bulk g-C₃N₄ was synthesized by polymerization of urea (NH₂CONH₂), while cetyl methyl ammonium bromide (CTAB) and AgNO₃ were the starting materials employed for the fabrication of Ag@AgBr hybrid. Ag@AgBr/g-C₃N₄ nanocomposite revealed stronger photocatalytic ability towards photo-degradation of MO and RhB. A diffraction peak at 38.1° attributed to metallic Ag was observed during XRD analysis. SEM and TEM analysis evaluated the morphological features of the Ag@AgBr/g-C₃N₄ composite. Fig. 7d displayed a platelet-like morphology of bulk g-C₃N₄, which provides more reactive sites for the growth of Ag@AgBr nanohybrids. Sphere-like Ag@AgBr hybrids with a particle

size of 200 nm were formed, and the platelet-like structure remains inviolate after Ag@AgBr particle growth on the g-C₃N₄ surface (Fig. 7e) (Yang et al., 2014).

Zhang *al.* constructed a novel VLT AgI/g-C₃N₄ photocatalyst using C₃H₆N₆, AgNO₃, potassium iodide (KI) and polyvinylpyrrolidone (PVP) as precursors with enhanced photocatalytic efficiency for diclofenac (DCF) removal (Zhang et al., 2017a). Murugesan et al. synthesized a VLD AgI/g-C₃N₄ nanocomposite via deposition precipitation method (Murugesan et al., 2018a).

2.3. Hydrothermal method

The hydrothermal approach is utilizing the chemical reaction among reagents at a particular temperature and pressure (Ghosh and Pal, 2019). Using a hydrothermal approach for facile preparation of AgX/g-C₃N₄ photocatalyst is an unusual approach. For example,

Akbarzadeh et al. employed bismuth (III) chloride (BiCl₃), ammonium metavanadate (NH₄VO₃), ethanolamine (C₂H₇NO), C₃H₆N₆ and AgNO₃ as precursors for the fabrication of g-C₃N₄/Ag/AgCl/BiVO₄ micro-flowers *viz.* one-pot hydrothermal treatment. Photocatalytic performance of as-prepared nanocomposite was examined for photo-removal of ibuprofen (IBF). To BiCl₃ solution, NH₄VO₃ was added to yield orange-coloured precipitates after that ethanolamine was added, and colour of the solution altered. Subsequently, the AgNO₃ solution was added to the above mixture via the precipitation-photodeposition method, and the whole solution was exposed under visible light in a photoreactor. The g-C₃N₄ solution was prepared and was consequently added to the above-prepared mixture by undergoing ultrasonication. The mixture was autoclaved and heated at 180 °C for 12 h, and then the obtained precipitates were dried to obtain

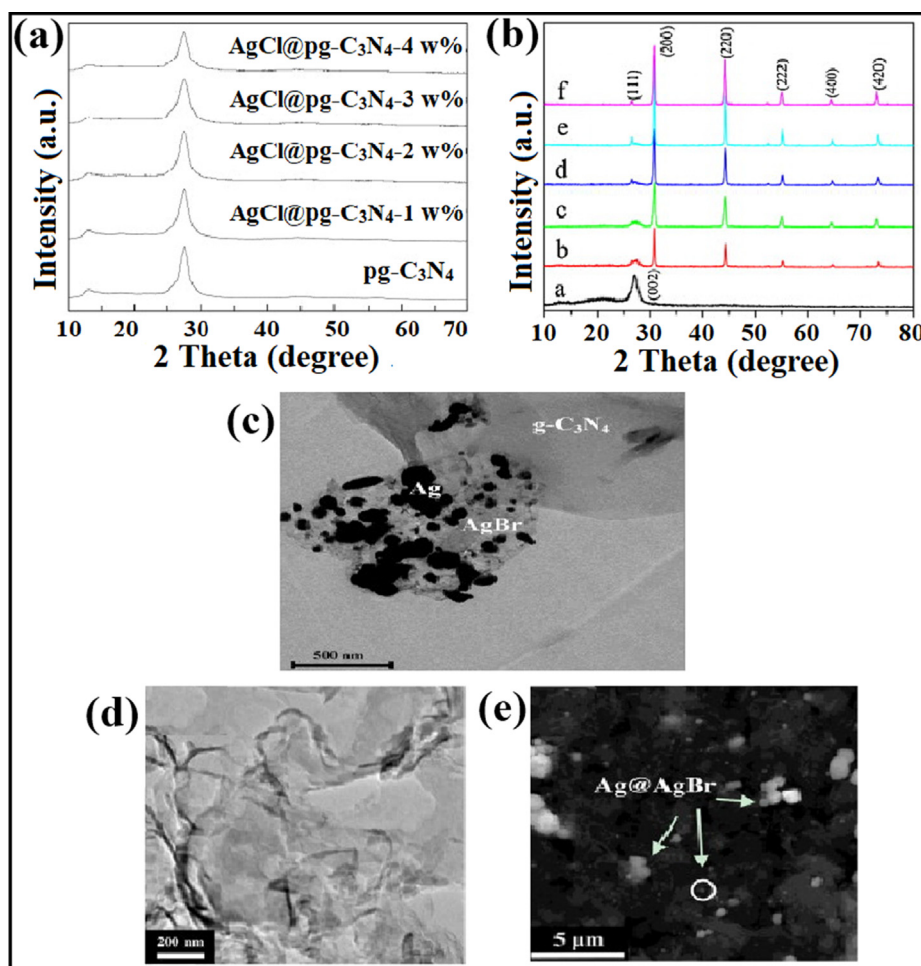


Fig. 7 (a) XRD analysis of as-prepared AgCl@pg-C₃N₄; reprinted with permission from Elsevier (Licence no. 4746510793950) (Mohamed, 2015), (b) XRD spectra of Ag/AgBr/g-C₃N₄ photocatalyst showing face-centered cubic assembly of AgBr, (c) TEM studies confirming the formation of as-synthesized nanocomposite; reprinted with permission from Elsevier (Licence no. 4746550937986) (Cao et al., 2013), TEM images demonstrating (d) platelet-like morphology of bulk g-C₃N₄, and (e) particle size of Ag@AgBr/g-C₃N₄ composite; reprinted with permission from Elsevier (Licence no. 4746561201233) (Yang et al., 2014).

g-C₃N₄/Ag/AgCl/BiVO₄ micro-flowers. XRD pattern (Fig. 8a) demonstrated a diffraction peak at 15.11°, which helped distinguish monoclinic scheelite BiVO₄ (m-BiVO₄) from tetragonal BiVO₄ (t-BiVO₄). While, peaks at 38.2° and 44.6° were attributed to metallic Ag, which indicated the photo-reduction of AgNO₃ from Ag⁺ to Ag⁰ (Akbarzadeh et al., 2018). Raizada and research group explored BiOBr/PSCN/Ag/AgCl Z-scheme photocatalytic mechanism for degradation of phenol under visible light, via a facile hydrothermal technique. SEM images (Fig. 8b) depicted the successful loading of BiOBr/Ag/AgCl NPs on phosphorus (P) and sulfur (S) co-doped g-C₃N₄ (PSCN) nanosheet (Raizada et al., 2020b).

Tang et al. investigated AgBr@g-C₃N₄/BiOBr via hydrothermal route followed by the *in-situ* ion-exchange method, utilizing NH₂CONH₂, KBr, ethylene glycol (EG) and AgNO₃ predecessors. The photocatalytic experimentations were carried out for RhB and tetracycline (TC) as target contaminants, under irradiation of visible light. Fig. 8c illustrated the detailed fabrication process of AgBr@g-C₃N₄/BiOBr nanoheterojunction. Fig. 8d explained SEM micrographs, which indicated the dispersal of AgBr particles on

g-C₃N₄/BiOBr composite (Tang et al., 2019a). Chen et al. studied 3D Ag/AgBr/g-C₃N₄@NGA Z-scheme based photocatalyst for efficient MO removal and antimicrobial activities were also investigated (Chen et al., 2019).

PGCN/AgI/ZnO/CQDs nanocomposite was developed by Hasija and co-workers employing NH₂CONH₂, diammonium hydrogen phosphate (NH₄)₂HPO₄, AgI, zinc nitrate tetrahydrate Zn(NO₃)₂, sodium hydroxide (NaOH), sodium iodide (NaI) and zinc oxide (ZnO) as starting material. While CQDs were prepared using bamboo leaves through facile hydrothermal treatment. SEM images confirmed the formation of PGCN/AgI/ZnO/CQDs nano-junction, as shown in Fig. 8e (Hasija et al., 2019c). Xue et al. studied g-C₃N₄/Bi₂WO₆/AgI nanocomposite following a Z-scheme photocatalytic system for efficient photodegradation of TC through hydrothermal reaction followed by *in-situ* precipitation method (Xue et al., 2019). Zhang et al. developed a VLD Z-scheme AgI/LaFeO₃/g-C₃N₄ photocatalyst for removal of norfloxacin (NOF) (Zhang et al., 2019).

During hydrothermal process, conditions of the reaction are very imperative. Solvent type, temperature as well as

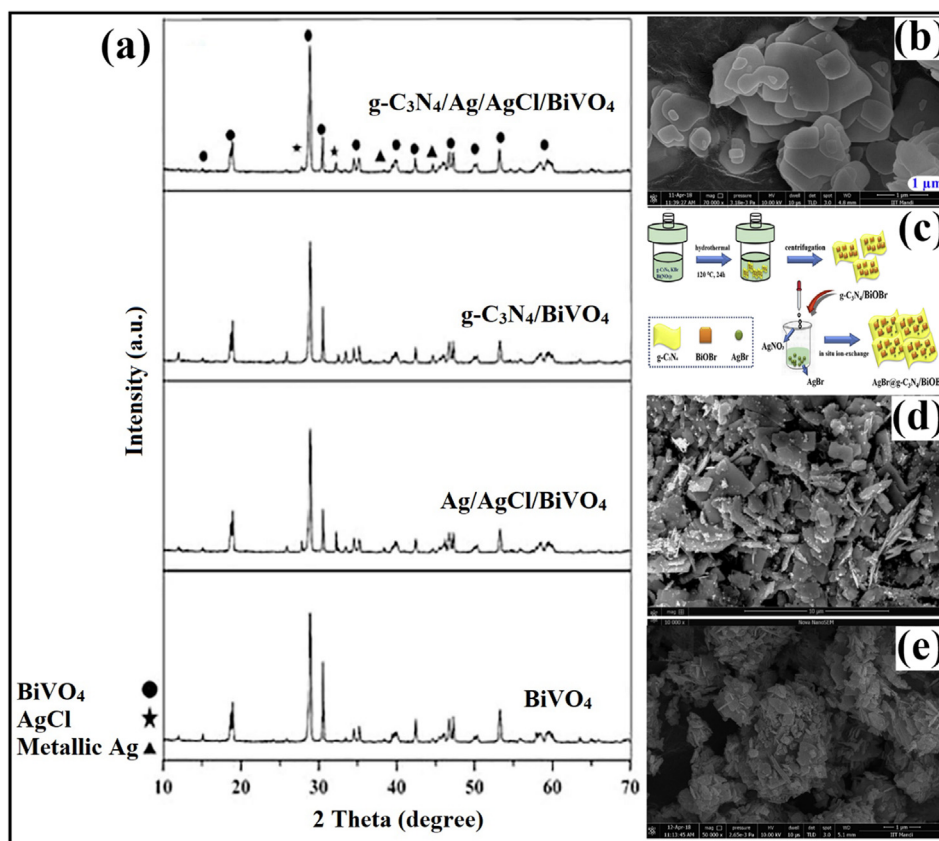


Fig. 8 (a) XRD pattern distinguishing monoclinic scheelite BiVO_4 from tetragonal BiVO_4 in $g\text{-C}_3\text{N}_4/\text{Ag}/\text{AgCl}/\text{BiVO}_4$ composite; reproduced with permission from Elsevier (Licence no. 4746601497828) (Akbarzadeh et al., 2018), (b) SEM images depicting successful loading of $\text{BiOBr}/\text{Ag}/\text{AgCl}$ NPs on PSCN nanosheet; reproduced with permission from Elsevier (Licence no. 4754600966798) (Raizada et al., 2019b), (c) Detailed fabrication process of $\text{AgBr}@g\text{-C}_3\text{N}_4/\text{BiOBr}$ nano-junction, (d) SEM imaginings revealing dispersal of AgBr particles on $g\text{-C}_3\text{N}_4/\text{BiOBr}$ composite; reproduced with permission from Elsevier (Licence no. 4746611095568) (Tang et al., 2019), and (e) SEM studies confirming formation of $\text{PGCN}/\text{AgI}/\text{ZnO}/\text{CQDs}$ heterostructure; reproduced with permission from Elsevier (Licence no. 4746620007509) (Hasija et al., 2019).

duration affect the synthesis of the products. Hydrothermal approach offers many advantages such as relatively mild operating conditions (reaction temperatures $< 300^\circ\text{C}$), one-step synthetic process, environmental friendly, and good dispersion in solution (Sōmiya and Roy, 2000). Besides, use of expensive autoclaves hinders its widespread applicability.

2.4. Ion-exchange method

An ion-exchange method is frequently employed for the synthesis of $\text{AgX}/g\text{-C}_3\text{N}_4$ composite. The operation circumstance is facile as well as lower in cost while choosing raw material is the crucial step in this scheme. For instance,

Zhang et al. employed $\text{C}_3\text{H}_6\text{N}_6$, AgNO_3 , EG, and hydrochloric acid (HCl) as precursor molecules for the synthesis of plasmonic $\text{Ag}@\text{AgCl}/g\text{-C}_3\text{N}_4$ photocatalyst *viz. in-situ* ion exchange process. The photocatalytic performance of as-fabricated nanocomposite was estimated for degradation of RhB, MO, MB, and phenols under natural light illumination. The detailed synthesis of $\text{Ag}@\text{AgCl}/g\text{-C}_3\text{N}_4$ nanocomposite was illustrated in Fig. 9a. TEM imaginings explained the black $\text{Ag}@\text{AgCl}$ hybrid with a particle size of $\sim 8\text{--}12$ nm was evenly dispersed on the surface of exfoliated $g\text{-C}_3\text{N}_4$ (Fig. 9b). XRD

analysis demonstrated the diffraction peaks for $\text{Ag}@\text{AgCl}/g\text{-C}_3\text{N}_4$, revealing face-centered cubic AgCl and peak intensities increased with increasing content of AgNO_3 (Zhang et al., 2014). A novel $\text{AgCl}/\text{Ag}_3\text{PO}_4/g\text{-C}_3\text{N}_4$ ternary composite was explored by Zhou and research group, with enhanced photocatalytic efficiency towards sulfamethoxazole (SMX) degradation (Zhou et al., 2017).

Tang et al. fabricated $g\text{-C}_3\text{N}_4/\text{Ag}_2\text{CO}_3/\text{AgBr}$ heterostructure by surface alteration of $g\text{-C}_3\text{N}_4/\text{Ag}_2\text{CO}_3$ thru AgBr NPs via the ion-exchange process. The synthesis process involved starting materials such as NH_2CONH_2 , sodium carbonate (Na_2CO_3), AgNO_3 , and NaBr . XRD pattern revealed the coexistence of Ag_2CO_3 and AgBr particles in the $g\text{-C}_3\text{N}_4/\text{Ag}_2\text{CO}_3/\text{AgBr}$ composite. The Fourier-transform infrared spectroscopy (FTIR) results confirmed the presence of NPs and the formation of heterojunction. Irregular and cubic AgBr particles were observed on polyhedral rod-like particles of Ag_2CO_3 , as explicated by SEM analysis (Fig. 9c) (Tang et al., 2017).

Tang and research group reported a Z-scheme based $g\text{-C}_3\text{N}_4/\text{Ag}_3\text{PO}_4/\text{AgI}$ nano-photocatalyst for evaluating the photocatalytic ability for nitenpyram (NTP) degradation. Fig. 9d explained the preparation method of $g\text{-C}_3\text{N}_4/\text{Ag}_3\text{PO}_4/\text{AgI}$

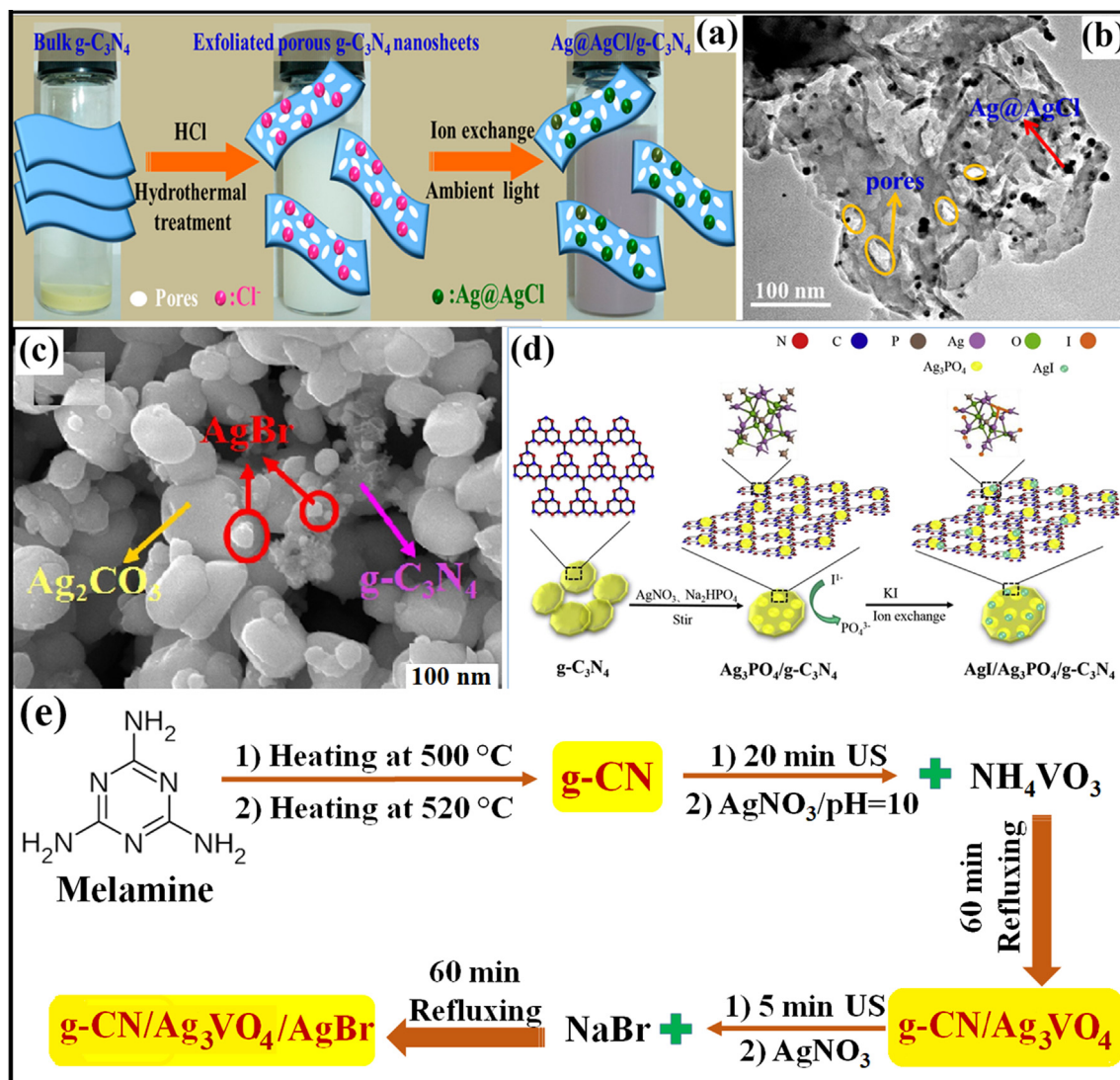


Fig. 9 (a) Fabrication of $\text{Ag@AgCl/g-C}_3\text{N}_4$ nanocomposite, (b) TEM imageries showing dispersal of black Ag@AgCl particles onto $g\text{-C}_3\text{N}_4$ surface; reprinted with permission from Elsevier (Zhang et al., 2014) (c) SEM analysis representing loading of cubic AgBr particles on rod-like particles of Ag_2CO_3 ; reprinted with permission from Elsevier (Licence no. 4746900302562) (Tang et al., 2017), (d) Synthesis scheme of $g\text{-C}_3\text{N}_4/\text{Ag}_3\text{PO}_4/\text{AgI}$ composite; reprinted with permission from Elsevier (Licence no. 4746910427726) (Tang et al., 2019), and (e) Preparation of $g\text{-CN}/\text{Ag}_3\text{VO}_4/\text{AgBr}$ nanocomposite (Barzegar et al., 2018).

nanocomposite through the *in-situ* ion-exchange route (Tang et al., 2019b).

Ion exchange method is widely employed in industrial scale for waste water treatment. The process is environmental friendly, has low maintenance cost and can provide high flow rate to treated water. Along with these benefits, certain limitations associated with this process are bacterial contamination, chlorine adulteration and adsorption of organic matter.

2.5. Refluxing method

Refluxing is a process involving condensation of vapours and the return of this condensate to the system from which it is originated. $g\text{-C}_3\text{N}_4/\text{Ag}_3\text{VO}_4/\text{AgBr}$ nanocomposites were studied by Barzegar et al. for the efficient elimination of toxins under visible light. The photocatalysts were synthesized by

loading Ag_3VO_4 and AgBr particles onto a $g\text{-C}_3\text{N}_4$ surface. Moreover, the detailed fabrication process can be observed in Fig. 9e and the solution was refluxed at 96°C for 1hr (Barzegar et al., 2018b).

Akhundi et al. reviewed $g\text{-C}_3\text{N}_4/\text{Fe}_3\text{O}_4/\text{AgI}$ nanocomposite by reflux method at 96°C (Akhundi and Habibi-Yangjeh, 2016c). A visible-light-driven $g\text{-C}_3\text{N}_4/\text{Ag}_2\text{CrO}_4/\text{AgI}$ photocatalyst was explored by Barzegar and co-workers via the refluxing process, for efficient photodegradation of RhB (Barzegar et al., 2018a). The typical process involved mixing of AgNO_3 (0.109 g) with a suspension containing 0.35 g of $g\text{-C}_3\text{N}_4/\text{AgCrO}$ (20%) sample. After that the sample was treated with 0.096 g of NaI and refluxed for 60 min at 96°C .

The method requires the use of relatively cheaper equipment's that are easy to operate and their setup is facile. Also, these methods are time consuming, involves the use of

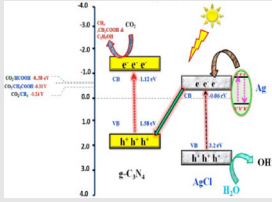
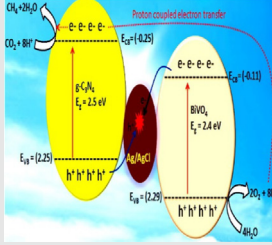
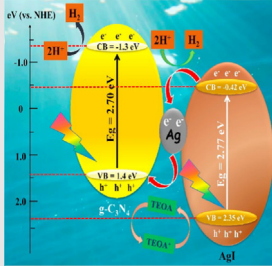
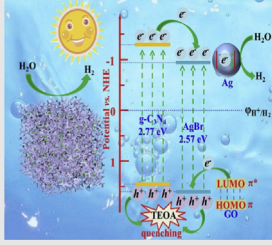
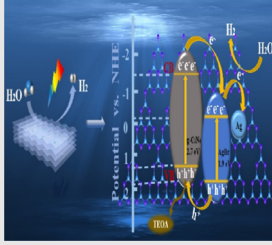
Table 1 Different AgX/g-C₃N₄ nanocomposites for pollutant degradation.

S. No.	Photocatalyst	Fabrication routes	Targeted Pollutant	Light source	Degradation Mechanisms	References
1.	Ag/AgCl/g-C ₃ N ₄	Facile preparation	MO	300 W Xe lamp with a 400 nm cut-off filter	—	Yang et al. (2014)
2.	g-C ₃ N ₄ /Fe ₃ O ₄ /AgCl	Facile preparation	RhB	50 W LED source		Akhundi and Habibi-Yangjeh (2015a)
3.	PoPD/AgCl/g-C ₃ N ₄	Photoinitiated polymerization method	TC	250 W Xe arc lamp		Sun et al. (2019)
4.	Ag/AgCl@ZIF-8/g-C ₃ N ₄	Facile stirring method	LVF	150 W Xe lamp equipped with 420 nm filter		Zhou et al. (2019)
5.	AgCl-Ag/g-C ₃ N ₄	Three step synthetic method	MO	350 W Xe lamp with UV cut-off filter ($\lambda > 420$ nm)		Yu et al. (2019)
6.	g-C ₃ N ₄ /AgCl/CDs	Impregnation method	MB, RhB	40 W LED bulb		Matheswaran et al. (2019)
7.	γ -Fe ₂ O ₃ /AgCl/g-C ₃ N ₄	Solvothermal and photodeposition method	Escherichia Coli (E. coli)	500 W tungsten halogen lamp		Ai et al. (2019)

Table 1 (continued)

S. No.	Photocatalyst	Fabrication routes	Targeted Pollutant	Light source	Degradation Mechanisms	References
8.	Ag/AgBr/ g-C ₃ N ₄	Solvothermal method	RhB	300 W Xe arc lamp equipped with ultraviolet cut filter		Xu and Zhang (2013)
9.	g-C ₃ N ₄ /GO/ AgBr	—	RhB	250 W Xe lamp with 420 nm cut-off filter		Miao et al. (2017b)
10.	Ag/AgBr/ V ₂ O ₅ /PCN	Hydrothermal method	Phenol	35 W LED lamp		Raizada et al. (2019b)
11.	g-C ₃ N ₄ / AgBr/rGO	—	2,4-dichlorophenol	250 W Xe lamp		Zhou et al. (2018)
12.	g-C ₃ N ₄ / Fe ₃ O ₄ /AgI/ Ag ₂ CrO ₄	Refluxing Method	RhB	50 W LED lamp		Akhundi and Habibi-Yangjeh (2016a)

Table 2 Different AgX/g-C₃N₄ nanocomposites for CO₂ photo-reduction and H₂ evolution.

Photocatalyst	Methodology	Process Conditions	Major products	Charge transfer mechanism	Quantum efficiency	Reference
AgCl@g-C ₃ N ₄	Deposition-precipitation method	11 W compact fluorescent lamp	Methane Acetic acid Formic acid		53.03 μmol g ⁻¹ 6.01 μmol g ⁻¹ 2.51 μmol g ⁻¹	Murugesan et al. (2018b)
g-C ₃ N ₄ /Ag/AgCl/BiVO ₄ (CAB)	Facile one-pot hydrothermal method	8 fluorescent lamps, 8 W each	Methane		205 μmol h ⁻¹ g ⁻¹	Rather et al. (2018)
AgBr/g-C ₃ N ₄ /NG (ACNNG)	Green and facile method	Xe arc lamp	Methanol Ethanol	—	105.89 μmol g ⁻¹ 256.45 μmol g ⁻¹	Li et al. (2015)
Ag/AgX (X = Cl, Br, I)/g-C ₃ N ₄	In-situ solid phase method	300 W Xe lamp	H ₂		Ag/AgCl/CN-4; 26.39 μmol g ⁻¹ h ⁻¹ Ag/AgBr/CN-4; 18.05 μmol g ⁻¹ h ⁻¹ Ag/AgI/CN-4; 59.22 μmol g ⁻¹ h ⁻¹	Bai et al. (2019)
PCN/GO/Ag/AgBr	Hard template method and selective chemical etching	300 W Xe lamp with a light filter of 420 nm	H ₂		3.69 mmol g ⁻¹ h ⁻¹	Li et al. (2019)
g-C ₃ N ₄ -Ag/AgBr (CNAA)	Solvothermal method	Xe lamp	H ₂		47.84 μmol g ⁻¹ h ⁻¹	Li et al. (2020)

flammable solvents and sometimes these techniques may be destructive limiting their practical implementations.

Tables 1 and 2 illustrates various other methods for fabrication of AgX coupled g-C₃N₄ nano-hybrids with different photocatalytic applications.

3. AgX/g-C₃N₄ nano-junctions

Amongst several semiconductor mediated nanostructures, construction of type-II and Z-scheme based heterojunctions

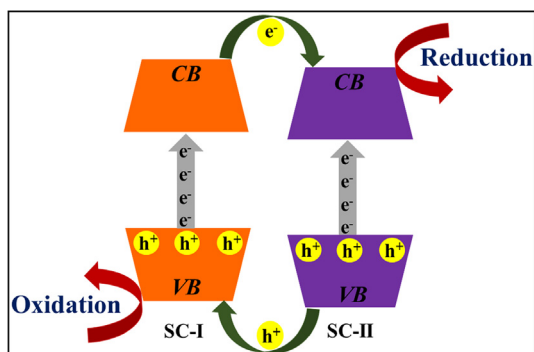


Fig. 10 Diagrammatic representation of type- II heterojunction.

have turned up as a facile way for elevating the photocatalytic efficacy.

3.1. Type-II heterojunctions

Combining two semiconducting materials where CB of semiconductor I (SC-I) is lower than that of semiconductor II (SC-II) and VB of SC-I has a higher value than that of SC-II, shown in Fig. 10. In type-II heterostructures, the band

potentials are positioned at optimum levels (staggered gap) that offer spatial charge carrier separation with enhanced photocatalytic efficacy. For instance, a novel work reporting deposition of AgCl NPs on the g-C₃N₄ surface was explored by Zhao et al. (2012). Shi and research group investigated AgCl decorated g-C₃N₄ (AgCl-CN), explicating the photodegradation process of oxalic acid (OA) under visible light irradiation. g-C₃N₄ and AgCl possess band gaps of 2.7 eV and 3.25 eV, respectively. Fig. 11a illustrated degradation mechanism explicating the transference of h_{VB}^+ of AgCl to VB of CN while CN e_{CB}^- shift to CB of AgCl. Therefore, photo-generated e_{CB}^- of AgCl ($E_{CB} = -0.06$ eV) reduces O₂ to produce $\cdot O_2^-$ due to its more negative reduction potential, while h_{VB}^+ of CN react with absorbed water to produce $\cdot OH$ radicals. These $\cdot O_2^-$ and $\cdot OH$ radicals were responsible for the photocatalytic degradation of OA (Shi et al., 2019).

Asadzadeh-Khaneghah et al. explicating the loading of carbon dots (CDs) and AgCl over the g-C₃N₄ network by a simple approach for the photocatalytic degradation of RhB, MB, MO, and phenol. g-C₃N₄-NS/CDs/AgCl photocatalyst with 20% of AgCl exhibited maximum photocatalytic activity. CDs acted as electron mediator amongst g-C₃N₄-NS and AgCl semiconductors. XRD analysis illustrated (Fig. 11b) that the introduction of CDs does not affect the assembly of g-C₃N₄ and no diffraction peaks were detected for CDs. Due to the

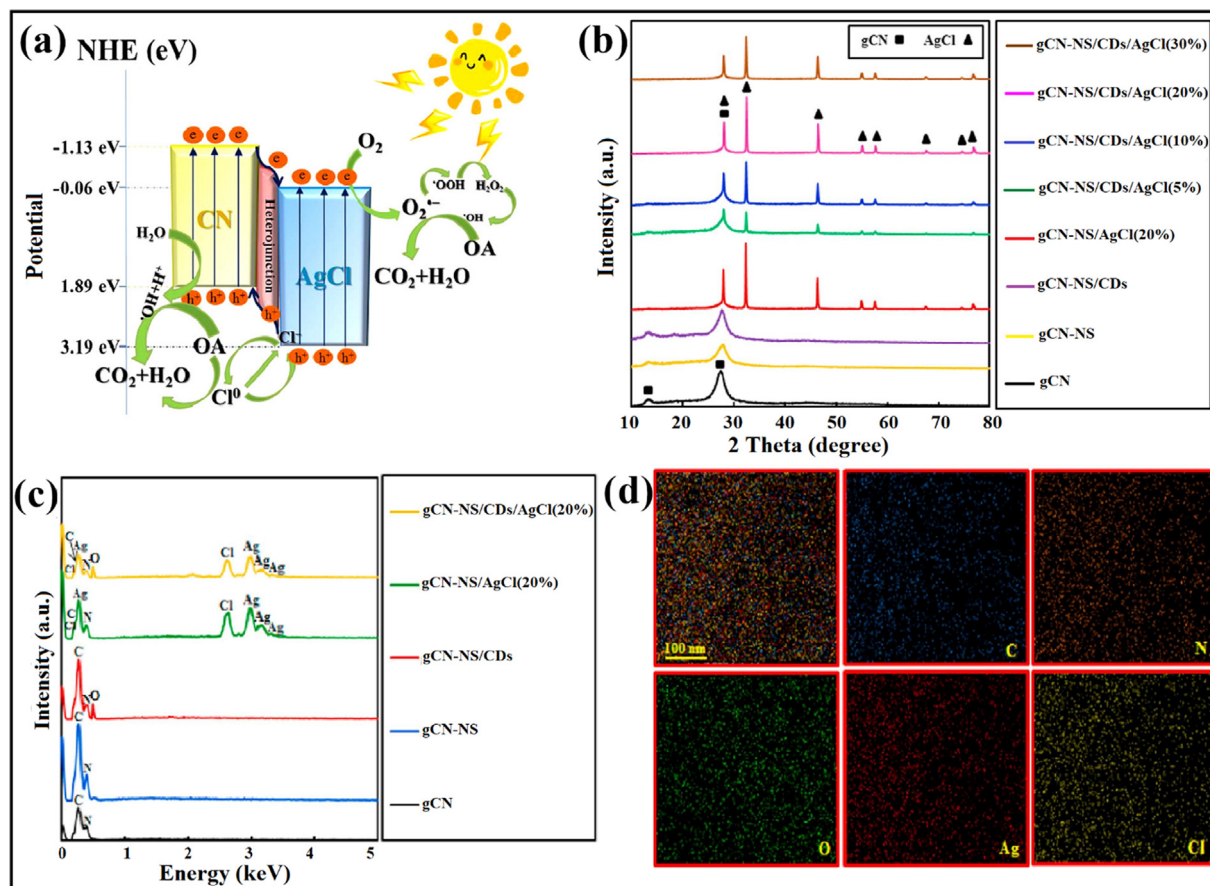


Fig. 11 (a) Type- II degradation mechanism in AgCl-CN nanocomposite; reproduced with permission from Elsevier (Licence no. 4747851498621) (Shi et al., 2019), (b) XRD pattern for g-C₃N₄-NS/CDs/AgCl photocatalyst with no prominent peaks for CDs, (c) EDX spectra of as-prepared nanocomposite, and (d) EDX mapping confirming elemental distribution; reprinted with permission from Elsevier (Licence no. 4747860423948) (Asadzadeh-Khaneghah et al., 2018).

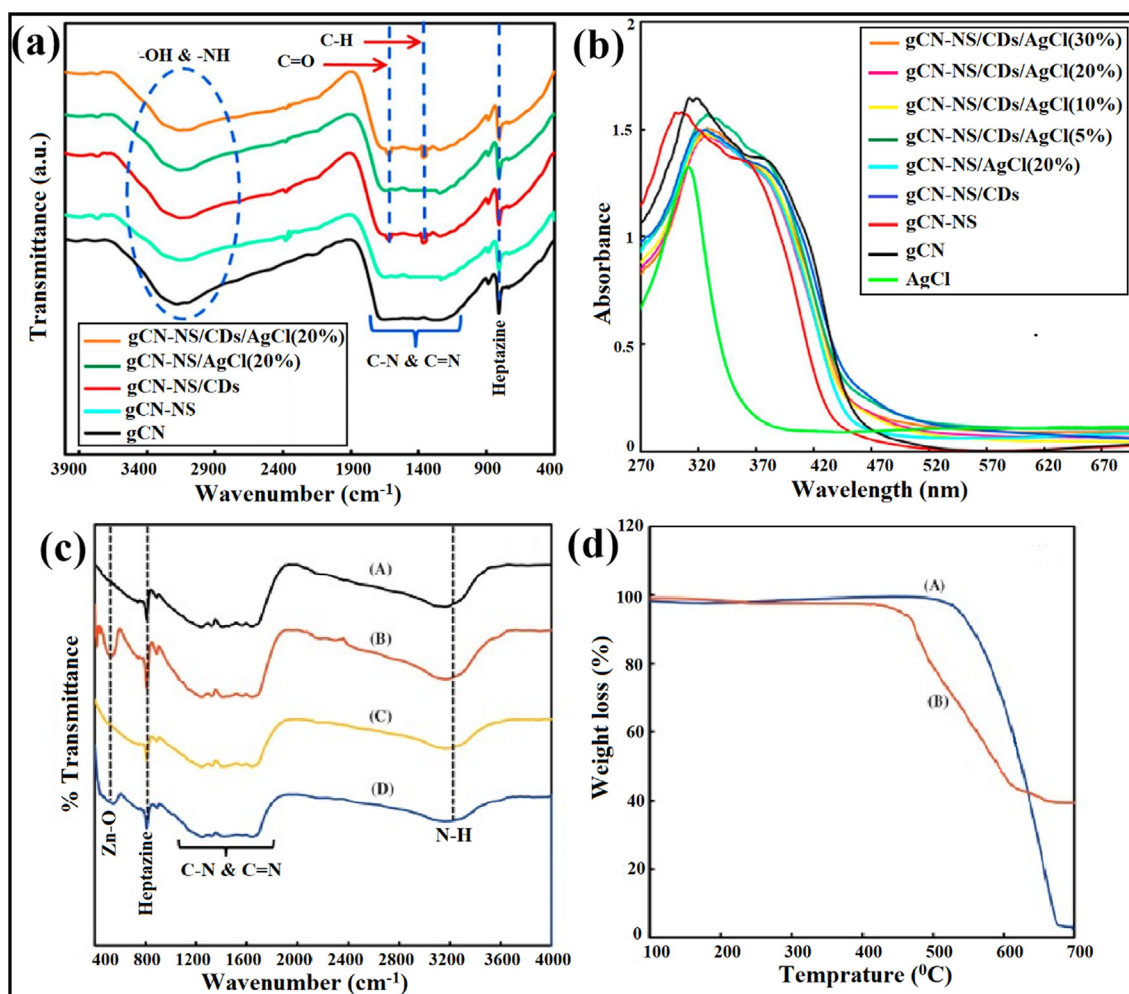


Fig. 12 $g\text{-C}_3\text{N}_4\text{-NS/CDs/AgCl}$ composite showing (a) FTIR analysis, (b) UV-visible spectra; reproduced with permission from Elsevier (Licence no. 4747860423948) (Asadzadeh-Khaneghah et al., 2018), (c) FTIR examinations confirming presence of Zn-O bond in $g\text{-C}_3\text{N}_4/\text{ZnO/AgCl}$ hybrid, and (d) TGA curves explicating the reduced weight of $g\text{-C}_3\text{N}_4$ (Akhundi et al., 2015); reproduced with permission from Elsevier (Licence no. 4747860921119).

existence of several functional groups such as hydroxyl, carbonyl, carboxyl, and epoxy in CDs, excessive amounts of oxygen elements were observed in Energy Dispersive X-ray (EDX) spectra (Fig. 11c). Fig. 11d explicated elemental distribution in $g\text{-C}_3\text{N}_4\text{-NS/CDs/AgCl}$ (20%) nanocomposite by EDX mapping. Further FTIR analysis demonstrated that exfoliation of $g\text{-C}_3\text{N}_4/\text{CDs}$ and integration of CDs and AgCl particles does not have any significant influence on the $g\text{-C}_3\text{N}_4$ structure. As well, no peak for the Ag-Cl bond was noticed, as observed in Fig. 12a. The exfoliated nature of $g\text{-C}_3\text{N}_4\text{-NS}$ was confirmed by the UV-DRS spectra, exhibiting a slight blue shift (Fig. 12b) (Asadzadeh-Khaneghah et al., 2018).

Akhundi and co-workers designed $g\text{-C}_3\text{N}_4/\text{ZnO/AgCl}$ ternary nano photocatalyst employing a facile methodology for the photocatalytic degradation process. Typically, $g\text{-C}_3\text{N}_4/\text{ZnO/AgCl}$ (40%) composite unveiled enhanced photocatalytic performance as compared to $g\text{-C}_3\text{N}_4/\text{ZnO}$ and $g\text{-C}_3\text{N}_4/\text{AgCl}$ nanocomposites. Further, FTIR studies (Fig. 12c) confirmed the presence of the ZnO sample with a characteristic peak at 540 cm^{-1} indexed to the Zn-O bond. Thermal gravimetric analysis (TGA) examinations (Fig. 12d) revealed that bulk

$g\text{-C}_3\text{N}_4$ lost its 97% of weight when heated up-to $700\text{ }^\circ\text{C}$ and decomposed to produce unsteady compounds. $g\text{-C}_3\text{N}_4/\text{ZnO/AgCl}$ nanocomposite loses its weight from about $420\text{ }^\circ\text{C}$ and lasts up-to $660\text{ }^\circ\text{C}$, while loading of ZnO/AgCl onto $g\text{-C}_3\text{N}_4$ sheet lead to decreased thermal stability. The photodegradation process of RhB was carried out at $25\text{ }^\circ\text{C}$ revealing 9% of RhB was photolyzed in 420 min under natural light illumination. 40% $g\text{-C}_3\text{N}_4/\text{ZnO/AgCl}$ composite exhibited maximum photocatalytic efficiency than pure $g\text{-C}_3\text{N}_4$, $g\text{-C}_3\text{N}_4/\text{ZnO}$, and $g\text{-C}_3\text{N}_4/\text{AgCl}$ composites. It was observed that about 39%, 46%, 58%, and 99% RhB was photodegraded in 270 min over $g\text{-C}_3\text{N}_4$, $g\text{-C}_3\text{N}_4/\text{ZnO}$, and $g\text{-C}_3\text{N}_4/\text{AgCl}$ and $g\text{-C}_3\text{N}_4/\text{ZnO/AgCl}$ (40%) samples, respectively. Approximately 6.7% (in dark) RhB molecules were adsorbed over as-synthesized composite after 420 min (Akhundi and Habibi-Yangjeh, 2015c). Lv and research group prepared $\text{Ag@AgCl}/g\text{-C}_3\text{N}_4/\text{TiO}_2$ ceramic films with superior photocatalytic abilities and a self-cleaning effect (Lv et al., 2018).

In another work, Miao and co-workers reported $g\text{-C}_3\text{N}_4/\text{AgBr}$ photocatalyst loaded with CDs for the photocatalytic removal of organic contaminants. $g\text{-C}_3\text{N}_4/\text{CDs/AgBr}$

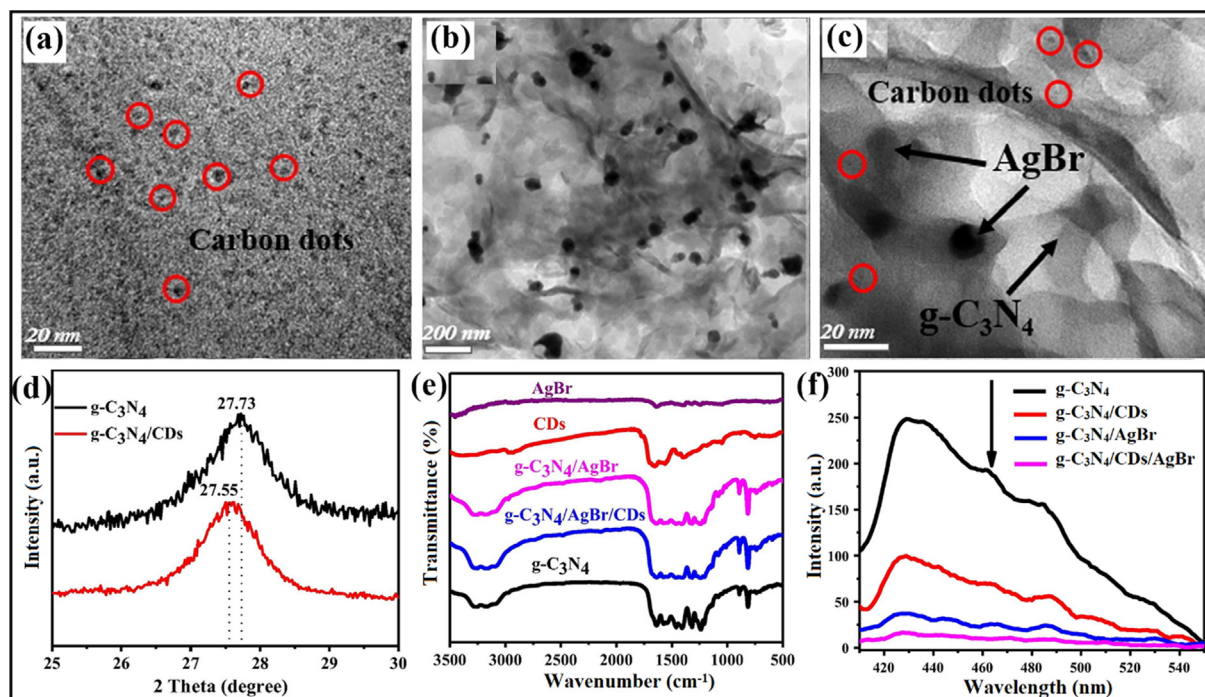


Fig. 13 $g\text{-C}_3\text{N}_4/\text{CDs}/\text{AgBr}$ nanocomposite presenting (a) TEM analysis of CDs, (b and c) TEM studies exhibiting loading of AgBr NPs on the surface of CDs modified $g\text{-C}_3\text{N}_4$ NS, (d) XRD pattern revealing shift of peaks by anchoring CDs into $g\text{-C}_3\text{N}_4$ sheet, (e) FTIR spectra describing no prominent peak for CDs, and (f) PL explorations of as-synthesized nanocomposite; reproduced with permission from Elsevier (Licence no. 4750670232021) (Miao et al., 2017).

photocatalyst revealed exceptional photocatalytic ability as comparable to pristine $g\text{-C}_3\text{N}_4$, AgBr, and $g\text{-C}_3\text{N}_4/\text{AgBr}$. Integration of CDs into $g\text{-C}_3\text{N}_4/\text{AgBr}$ amended the photocatalytic efficacy due to light-absorbing and electron sinking nature of CDs amongst $g\text{-C}_3\text{N}_4$ and AgBr. TEM analysis clarified the size of CDs which was found to be 5 nm (Fig. 13a) and loading of AgBr NPs on the surface of CDs modified $g\text{-C}_3\text{N}_4$ NS was shown in Fig. 13b and c. XRD pattern explained the incorporation of CDs into $g\text{-C}_3\text{N}_4$ causing a shift of peaks with a slight distortion of the $g\text{-C}_3\text{N}_4$ lattice, as shown in Fig. 13d. Moreover, the FTIR examination described that no prominent peak for CDs was noticed in $g\text{-C}_3\text{N}_4/\text{CDs}/\text{AgBr}$ nanocomposite (Fig. 13e). As reported earlier, Brunauer-Emmett-Teller (BET) specific surface area of $g\text{-C}_3\text{N}_4/\text{CDs}$ ($68.20\text{ m}^2/\text{g}$) was higher than that of pristine $g\text{-C}_3\text{N}_4$ ($57.09\text{ m}^2/\text{g}$), demonstrating that addition of $g\text{-C}_3\text{N}_4$ lead to the boosted surface area. Consequently, it offers more reactive sites for adsorption and catalysis processes. Photoluminescence (PL) examinations (Fig. 13f) revealed that integration of CDs or AgBr onto $g\text{-C}_3\text{N}_4$ sheet inhibits the spatial charge separation of photo-induced charge carriers. Moreover, the photocatalytic ability of nanocomposite was enhanced, and insertion of CDs lessened the recombination of photo-induced EHP (Miao et al., 2017a).

Chen et al. explored Ag/AgBr/ $g\text{-C}_3\text{N}_4$ photocatalyst by a facile technique with greater photocatalytic ability for elimination of MB. The optimum Ag/AgBr content with maximum photocatalytic efficiency was determined to be 40%. The efficacious photocatalytic ability could be allocated to extended visible light absorption and effective spatial charge separation due to the SPR effect of Ag^0 . Ag/AgBr particles own

sphere-like morphology with a particle size of 500 nm (Fig. 14a), and the intercalation of AgBr particles into $g\text{-C}_3\text{N}_4$ layers was explained in SEM images. With increased AgBr content, bigger AgBr particles were obtained and assembled instantaneously. Ag/AgBr NPs ranging from 50 nm to 200 nm were well distributed onto $g\text{-C}_3\text{N}_4$ sheet, deprived of noticeable accumulation. Fig. 14b explained that several Ag crystals with a particle size of 10 nm appeared along with AgBr particle. X-ray photoelectron spectroscopy (XPS) studies determined the elemental composition of as-synthesized composite. XPS peaks confirm that Ag/AgBr/ $g\text{-C}_3\text{N}_4$ powders comprised of Ag, Br, O, N, and C elements and with the element content of 2.81%, 1.8%, 3.77%, 42.68%, and 48.93%, respectively. The diffraction peaks at 366.8 eV and 372.8 eV were allocated to Ag^+ in AgBr, and the peaks at 374.5 eV and 368.5 eV were indexed to Ag^0 , as illustrated in Fig. 14c. Ag/AgBr/ $g\text{-C}_3\text{N}_4$ nanocomposite displayed significant improvement of light absorption at wavelengths 500–900 nm (Fig. 14d), and upon aggregating the Ag/AgBr content absorption intensities improved, which could be indexed to the SPR effect of Ag nanocrystals. The improved photocatalytic ability of Ag/AgBr/ $g\text{-C}_3\text{N}_4$ composite may be due to the synergetic effect of Ag, AgBr, and $g\text{-C}_3\text{N}_4$, as shown in. At the same time, metallic Ag on AgBr surface plays a crucial role in e^- transformation (Cao et al., 2013). The band potentials of $g\text{-C}_3\text{N}_4$ and AgBr were 2.7 eV and 2.6 eV, respectively, with more negative CB energies of $g\text{-C}_3\text{N}_4$ (-1.12 eV), than that of AgBr (-0.3 eV) and more positive VB energies of AgBr ($+2.3\text{ eV}$), than that of $g\text{-C}_3\text{N}_4$ ($+1.58\text{ eV}$). Therefore, photo-induced e_{CB}^- easily gets transferred from $g\text{-C}_3\text{N}_4$ to CB of AgBr, thereby producing CO_2 by reacting with adsorbed O_2 . Meanwhile,

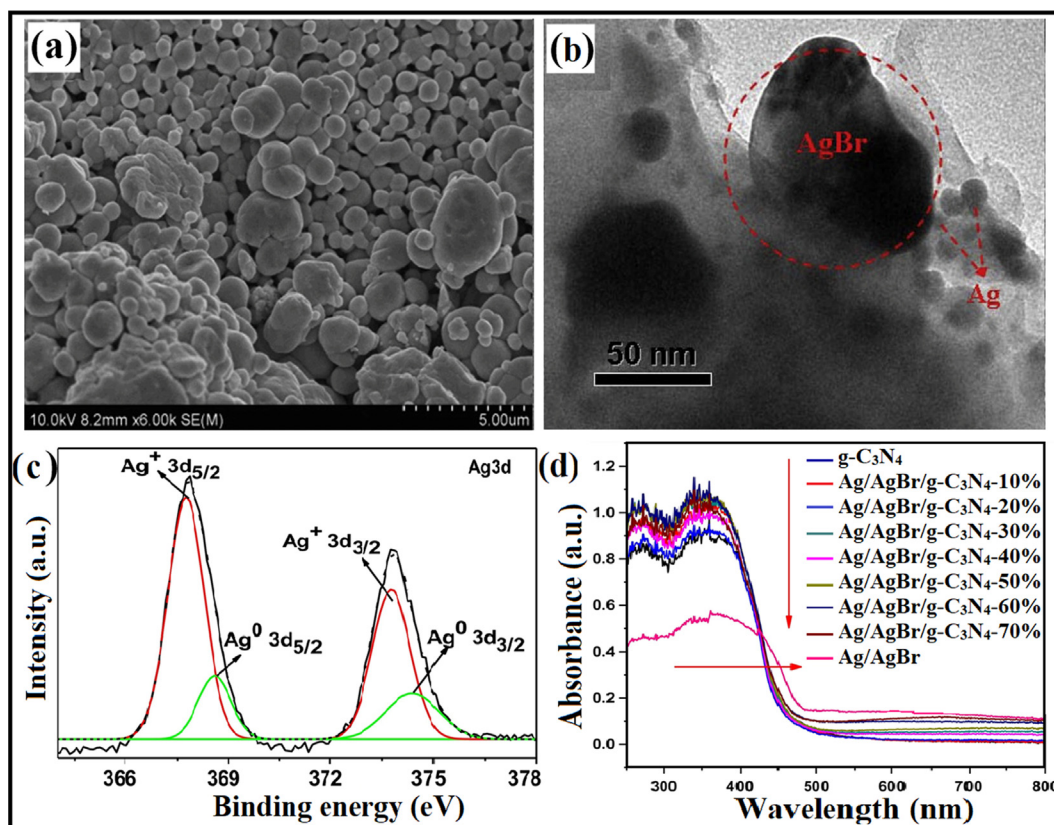


Fig. 14 (a, b) SEM images of Ag/AgBr/g-C₃N₄ photocatalyst, (c) XPS examination revealing existence of Ag⁺ in AgBr, and (d) UV-Visible analysis of as-fabricated photocatalyst; reprinted with permission from Elsevier (Licence no. 4746461343390) (Chen et al., 2015).

photo-induced $h\nu_{\text{VB}}^+$ of AgBr relocates to the surface of g-C₃N₄. Furthermore, metallic Ag can provide photo-induced e^- accredited to SPR effect, and Fermi level of AgBr lies inferior to that of Ag, consequently e^- transfer from Ag to AgBr and lastly transferred to adsorbed O₂ to generate $\cdot\text{O}_2^-$ (Chen et al., 2015a). Another work was explored by Akhundi and co-workers reporting the construction of g-C₃N₄/AgBr/Fe₃O₄ nano-composite with enhanced photocatalytic performance (Akhundi and Habibi-Yangjeh, 2015b). Mousavi et al. investigated a VLT magnetically recoverable g-C₃N₄/Fe₃O₄/Ag₂-WO₄/AgBr quaternary photocatalyst for photodegradation of contaminants (Mousavi and Habibi-Yangjeh, 2018b).

Liu et al. reported AgI@g-C₃N₄ core-shell structures for efficient degradation of MB dye under the illumination of visible light (Liu et al., 2015). AgI/g-C₃N₄ nanocomposite was prepared by Lei and group, while TEM images (Fig. 15a) explicated that AgI NPs were stacked on g-C₃N₄ surface with increasing AgI content and particle size of AgI was observed to be about 30 nm (Lei et al., 2016). Akhundi and his research group explored recyclable g-C₃N₄/Fe₃O₄/AgI photocatalyst with superior photocatalytic activity for removal of RhB via the reflux method at 96°. The g-C₃N₄/Fe₃O₄/AgI (20%) composite illustrated more exceptional photocatalytic ability than bulk g-C₃N₄ and g-C₃N₄/Fe₃O₄ samples. XRD spectra for g-C₃N₄/Fe₃O₄/AgI nanocomposites revealed that diffraction peaks for AgI were associated to hexagonal crystal phase (Fig. 15b). SEM experimentations explained the loading of Fe₃O₄ and AgI particles on g-C₃N₄ sheet. Also, particle size was observed to be about 30 nm, as shown in Fig. 15c. Moreover, no peak for the Ag-I bond was observed, as illustrated by

FTIR studies. Fig. 15d depicted two typical peaks at 430 and 620 cm⁻¹ attributed to the Fe-O bond. The mechanistic view for g-C₃N₄/Fe₃O₄/AgI nanocomposite explicated the excitation of e^- from VB to CB under visible light illumination. Attributable to confined band gaps of g-C₃N₄ and AgI, the e_{CB}^- reacts with adsorbed O₂ to generate H₂O₂, and these H₂O₂ molecules produced $\cdot\text{OH}$ radicals by e^- capturing. Though VB of g-C₃N₄ does not produce $\cdot\text{OH}$ radicals owing to lower VB energies of g-C₃N₄ (+1.58 eV) than adsorbed $\cdot\text{OH}$ ($E_{\text{OH}/\cdot\text{OH}}^\circ = +2.38$ eV) and H₂O ($E_{\text{H}_2\text{O}}^\circ = +2.72$ eV). The O₂, $\cdot\text{O}_2^-$ and h^+ produced were the reactive species (RSs) accountable for photodegradation of RhB, as shown in Fig. 15e (Akhundi and Habibi-Yangjeh, 2016c).

3.2. Z-scheme based heterojunctions

Z-scheme heterojunction possesses more negative CB potentials and more positive VB potentials, thereby lowering the bandgap of the semiconductor. In Z-scheme arrangements, under natural light illumination, e_{CB}^- of SC-II merge with photo-generated $h\nu_{\text{VB}}^+$ of SC-I, as illustrated in Fig. 16. This caused the formation of sufficiently strong oxidative $h\nu_{\text{VB}}^+$ in SC-II and reductive e_{CB}^- of SC-I. This induced interface electric field accelerates the separation of EHP. For example, Zhou and co-workers investigated a plasmonic Ag/AgCl/g-C₃N₄ Z-scheme nano photocatalyst by an *in-situ* oxidation process. Ag/AgCl/g-C₃N₄ with an Ag/AgCl amount of 2.7 at % attained a more exceptional photocatalytic ability for mineralization of MO. TEM study demonstrated the dispersal of Ag NPs on the flake-like structure of g-C₃N₄, with a particle size

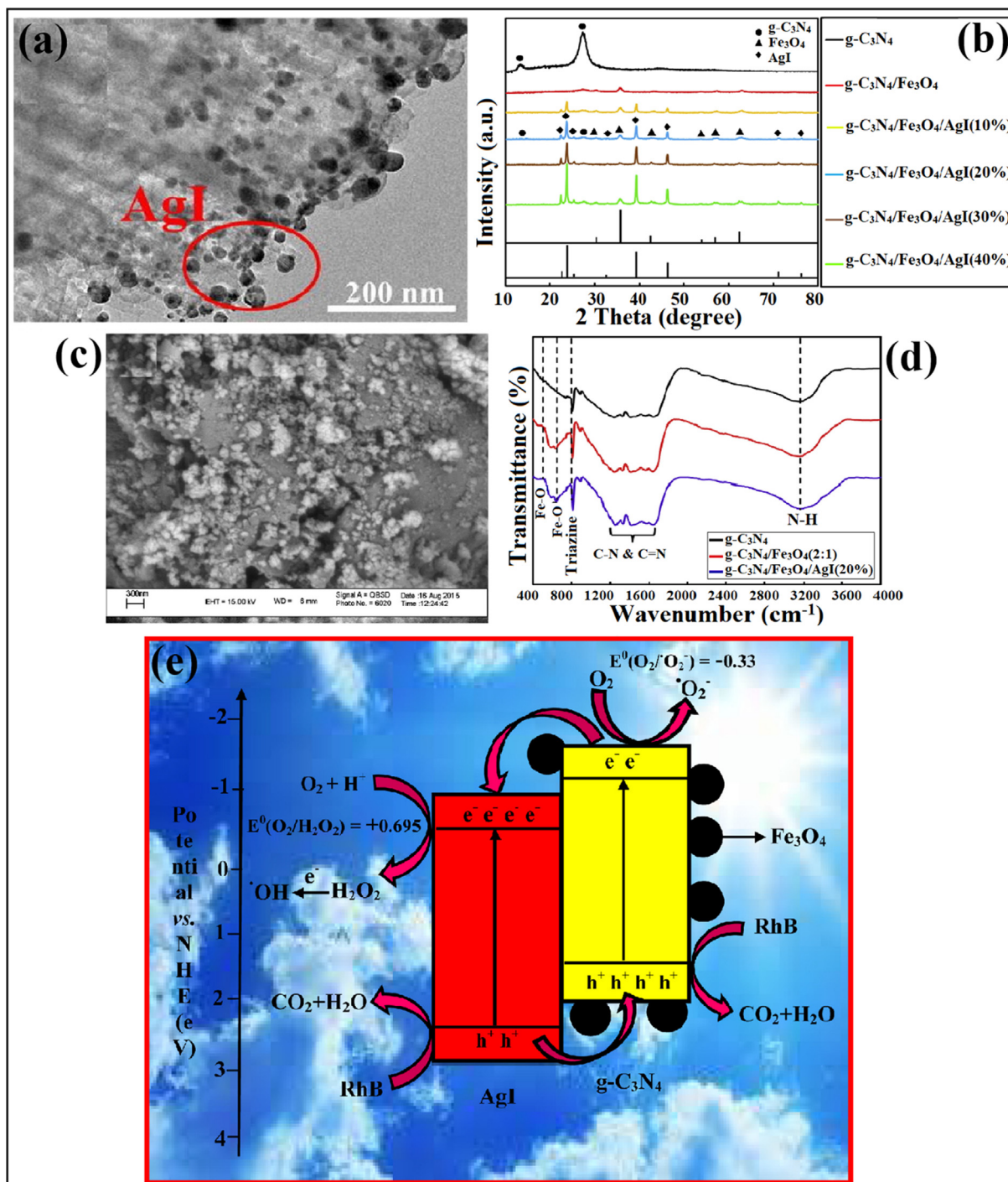


Fig. 15 (a) TEM imaginings of AgI/g-C₃N₄ nanocomposite; reproduced with permission from Elsevier (Licence no. 4750100779496) (Lei et al., 2016), (b) XRD pattern of g-C₃N₄/Fe₃O₄/AgI nano-hybrid, (c) SEM analysis explained loading of Fe₃O₄ and AgI particles on g-C₃N₄ sheet, (d) FTIR studies confirming Fe-O bond, and (e) Photocatalytic degradation mechanism of as-prepared photocatalyst; reproduced with permission from Elsevier (Licence no. 4750110390251) (Akhundi and Habibi-Yangjeh, 2016).

of 10–50 nm, as shown in Fig. 17a. Consistent with Fig. 17b g-C₃N₄ acted as template for dispersion of Ag/AgCl crystals due to which agglomeration reduced and interface among Ag/AgCl augmented. No covalent bond was noticed amongst Ag/AgCl and g-C₃N₄, and the deposition of Ag/AgCl on the g-C₃N₄ surface was demonstrated by FTIR analysis, Fig. 17c. As per

photocurrent examinations, the transient photocurrent response of Ag/AgCl/g-C₃N₄ composite is greater than that of bare g-C₃N₄, which means higher separation efficacy of EHP could be achieved, as illustrated in Fig. 17d (Zhou et al., 2014). Li et al. Ag@AgCl QDs decorated g-C₃N₄ nano-plates *viz.* oil-in-water self-assembly process (Li et al.,

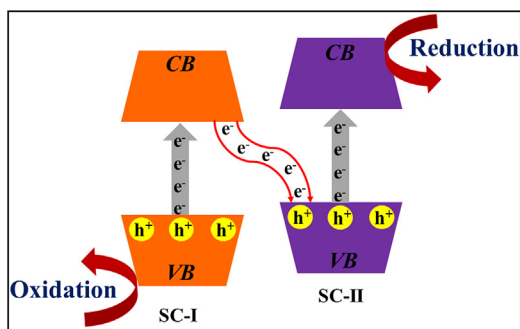


Fig. 16 Diagrammatic representation of Z-scheme based heterojunction.

2017). Bao et al. explored a plasmonic AgCl/Ag/g-C₃N₄ composite ascribed to Z-scheme based mechanism, presented in Fig. 17e. Therefore, under exposure to solar light, both Ag and g-C₃N₄ get excited, thus producing photo-induced EHP. The photo-illuminated e⁻ of Ag NPs travel to CB of AgCl to reduce O₂. In the meantime, photo-induced e⁻ of g-C₃N₄ go to Ag NPs to recombine with photo-generated h⁺ that were created by plasmonic absorption of Ag NPs. While the plasmon-induced h_{VB}⁺ of g-C₃N₄ reduces the organic pollutant (Bao and Chen, 2016).

A Z-scheme Ag@AgBr grafted graphitic carbon nitride (Ag@AgBr/g-C₃N₄) by photo reducing AgBr/g-C₃N₄ nanohybrids was fabricated by deposition-precipitation process. The photocatalytic proficiency of the prepared sample was explored for the photo-degradation of MO and RhB dye. Under solar light irradiation, e_{VB}⁻ of both g-C₃N₄ and AgBr were excited to vacant CB producing EHP, respectively. As a result of more negative CB edges of AgBr (-0.3 V) comparable to fermi level of Ag (0.4 V), e⁻ in CB of AgBr can simply migrate into Ag metal through Schottky barrier. Since the VB edge of g-C₃N₄ (1.4 V) is more favourable than the fermi level of Ag, therefore, e⁻ from Ag travel to VB of g-C₃N₄. Subsequently, a Z-scheme mechanism was proposed, as shown in Fig. 18a. Accordingly, e_{CB}⁻ of g-C₃N₄ reacts with O₂ forming O₂⁻ radicals while h_{VB}⁺ of AgBr travel onto the surface forming Br⁰ atoms. O₂⁻ and Br⁰ were the RSs accountable for the photodegradation of MO (Yang et al., 2014). In another work, Feng et al. constructed a g-C₃N₄/AgBr photocatalyst and concluded that integration of AgBr hybrid on g-C₃N₄ NS results in the formation of heterostructures, as elucidated by electrochemical impedance spectroscopy (EIS) Nyquist plots. A reduced arc radius of the EIS Nyquist plot reflects greater charge transference befalling at the interface. Owing to a smaller arc radius of as-prepared samples, these revealed more efficient spatial separation of plasmon-induced charge carriers (Feng et al., 2015). Azimi et al. proposed a ternary g-C₃N₄/AgBr/ZnO nanocomposite for active degradation of MB dye (Azimi et al., 2018).

Xue et al. explored a ternary g-C₃N₄/Bi₂WO₆/AgI Z-scheme photocatalytic system with improved photocatalytic activity towards the exclusion of TC. TEM analysis (Fig. 18b) depicted the microspheres of Bi₂WO₆, and it was observed that AgI NPs were unevenly deposited on g-C₃N₄ surface, with the existence of an active link among g-C₃N₄, AgI as well as Bi₂WO₆. Fig. 18c illustrated the proposed mechanism for

photodegradation of organic pollutants. Under visible light excitation, the photo-illuminated e_{CB}⁻ of Bi₂WO₆ recombines with h_{VB}⁺ of g-C₃N₄ and AgI, resulting in spatial charge separation of photo-induced EHP. The transference of photo-charge carriers leads to retaining of e⁻ at CB of g-C₃N₄ and AgI, while h⁺ remains accumulated at the VB of Bi₂WO₆, respectively. Owing to more negative CB energies of g-C₃N₄ (-0.913 eV) and AgI (-0.503 eV) than O₂/⁻O₂ (-0.33 eV vs. NHE), the photo-induced e_{CB}⁻ of g-C₃N₄ and AgI could reduce O₂ to ⁻O₂. Moreover, photo-induced h⁺ of Bi₂WO₆ can activate H₂O molecules to produce [•]OH due to less negative VB potential of Bi₂WO₆ (3.147 eV) than that of H₂O/[•]OH (+2.72 eV) (Xue et al., 2019). A dual Z-scheme g-C₃N₄/Ag₃PO₄/AgI photocatalyst with improved photocatalytic ability for removal of neonicotinoid pesticide, was explored (Tang et al., 2019b). In other work, Zhang et al. fabricated a ternary photocatalyst with greater photocatalytic activities for the elimination of NOF (Zhang et al., 2019).

4. Multifunctional applications

4.1. Reduction of carbon dioxide (CO₂) to useful hydrocarbon fuels

A novel Z-scheme AgCl@g-C₃N₄ nanocomposite was fabricated via deposition-precipitation routes, thereby, loading different ratios of AgCl on g-C₃N₄ surface. The photocatalytic ability of as-prepared sample was investigated under visible light eradication for CO₂ reduction in an aqueous medium (Fig. 19a). The VB and CB potentials for g-C₃N₄ were located at +1.58 eV and -1.12 eV, correspondingly, while for AgCl, these are located at 3.2 eV and -0.06 eV, respectively. As a result of a broad bandgap, AgCl (~3.26 eV) could not absorb visible light. Attributable to the LSPR effect, Ag⁰ NPs absorb visible light, thereby producing EHP. Consequently, photo-generated e⁻ can migrate from Ag⁰ NPs to AgCl hybrid. Thus the accumulated particles in AgCl CB cannot photo-reduce CO₂ to methane (CH₄), acetic acid (CH₃COOH), and formic acid (HCOOH). Since, CB potentials of AgCl (-0.06 eV vs. NHE) is more favourable than the typical redox potential of CO₂ to CH₄ (-0.24 V vs. NHE), CH₃COOH (-0.31 V) and HCOOH (-0.58 V vs. NHE). The accumulated e⁻ on the surface of AgCl can directly associate with the h_{VB}⁺ of g-C₃N₄. The spatial charge separation of photo-illuminated EHP does not follow a conservative double-transferral approach. Therefore, a possible Z-scheme mechanism for the reduction process has been suggested. The surface e⁻ of AgCl directly associates with h_{VB}⁺ of g-C₃N₄. Meanwhile, the photo-generated e_{CB}⁻ of g-C₃N₄ (-1.12 eV) could react with adsorbed CO₂ to reduce CH₄, CH₃COOH, and HCOOH. It can be inferred that the Z-scheme charge transference path in AgCl@g-C₃N₄ nanocomposite can effectually lower the recombination of photo-charge carriers (Murugesan et al., 2018b).

Rather et al. explored g-C₃N₄/Ag/AgCl/BiVO₄ (CAB) composite for photo-reduction of CO₂ to CH₄ under alkali activation. The morphology of the CAB microstructure was reliant on anchoring of AgNO₃ and g-C₃N₄, as explained by SEM studies. Pristine BiVO₄ and g-C₃N₄ own sheet-like structure, while Ag/AgCl nanocrystals were formed by deposition of Ag⁰ and precipitation of AgCl onto BiVO₄. The XPS spectra revealed the existence of all probable elements in the

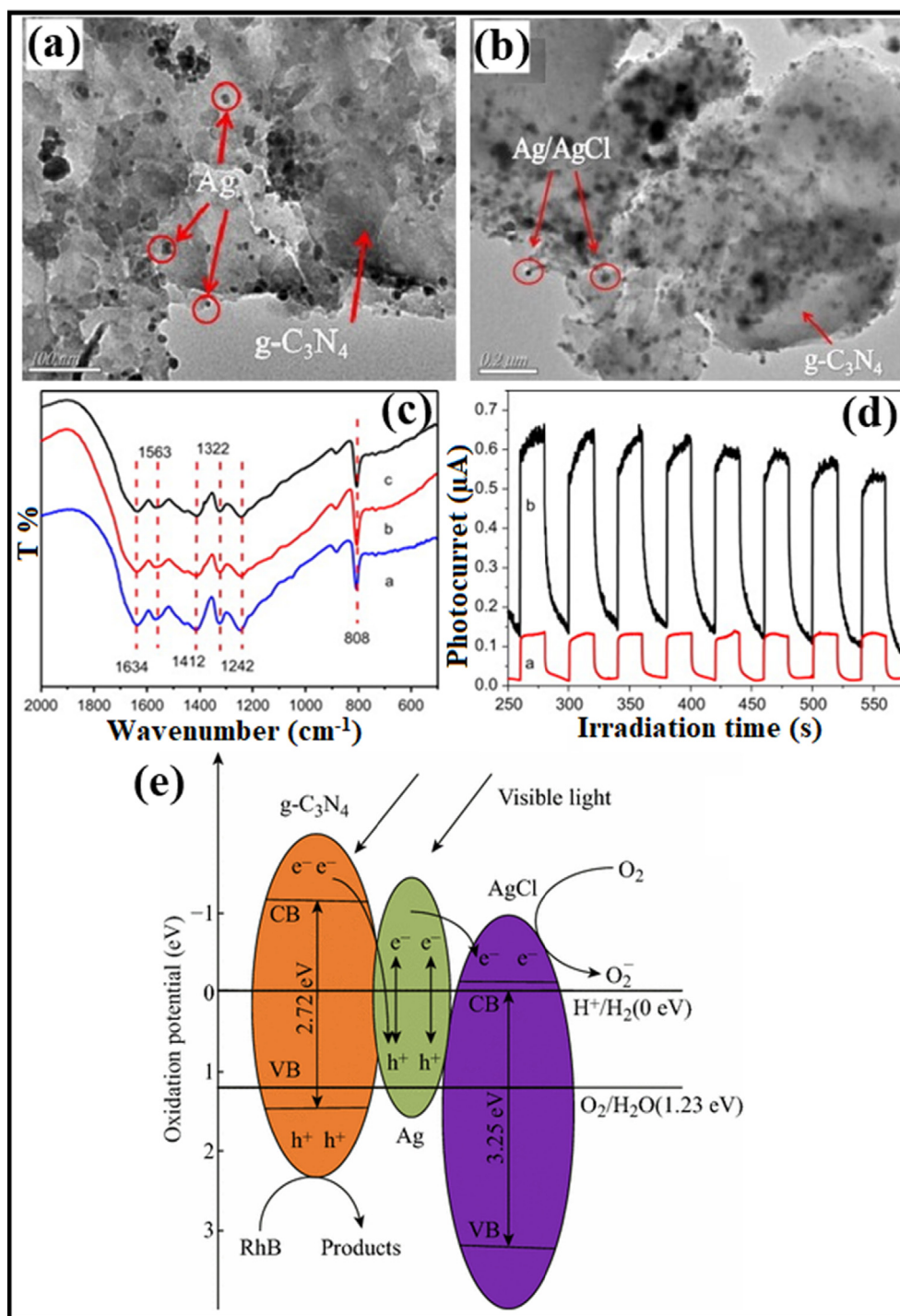


Fig. 17 (a and b) TEM imageries of Ag/AgCl/g-C₃N₄ photocatalyst, (c) FTIR investigations of as-synthesized composite, (d) Photocurrent analysis depicting higher separation efficacy of EHP; reprinted with permission from Elsevier (Licence no. 4750660226117) (Zhou et al., 2014), and (e) Z-scheme photocatalytic mechanism of AgCl/Ag/g-C₃N₄ composite; reprinted under licence from CC BY 4.0 (Bao and Chen, 2016).

g-C₃N₄/Ag/AgCl/BiVO₄ microstructure. The chemical shift near reduced binding energies was perceived after achieving the photocatalytic CO₂ reduction, and downshift was observed because of the integration of sodium (Na) after alkali treatment. The interfacial possessions of the nanocomposite were

scrutinized by observing their photoelectrochemical cell (PEC) response employing linear sweep voltammetry (LSV) technique mutually in the existence and nonexistence of light. CAB-1 (5.03 mA cm⁻¹) and g-C₃N₄-BiVO₄ (4.1 mA cm⁻²) witnessed small currents in the absence of light, succeeded by

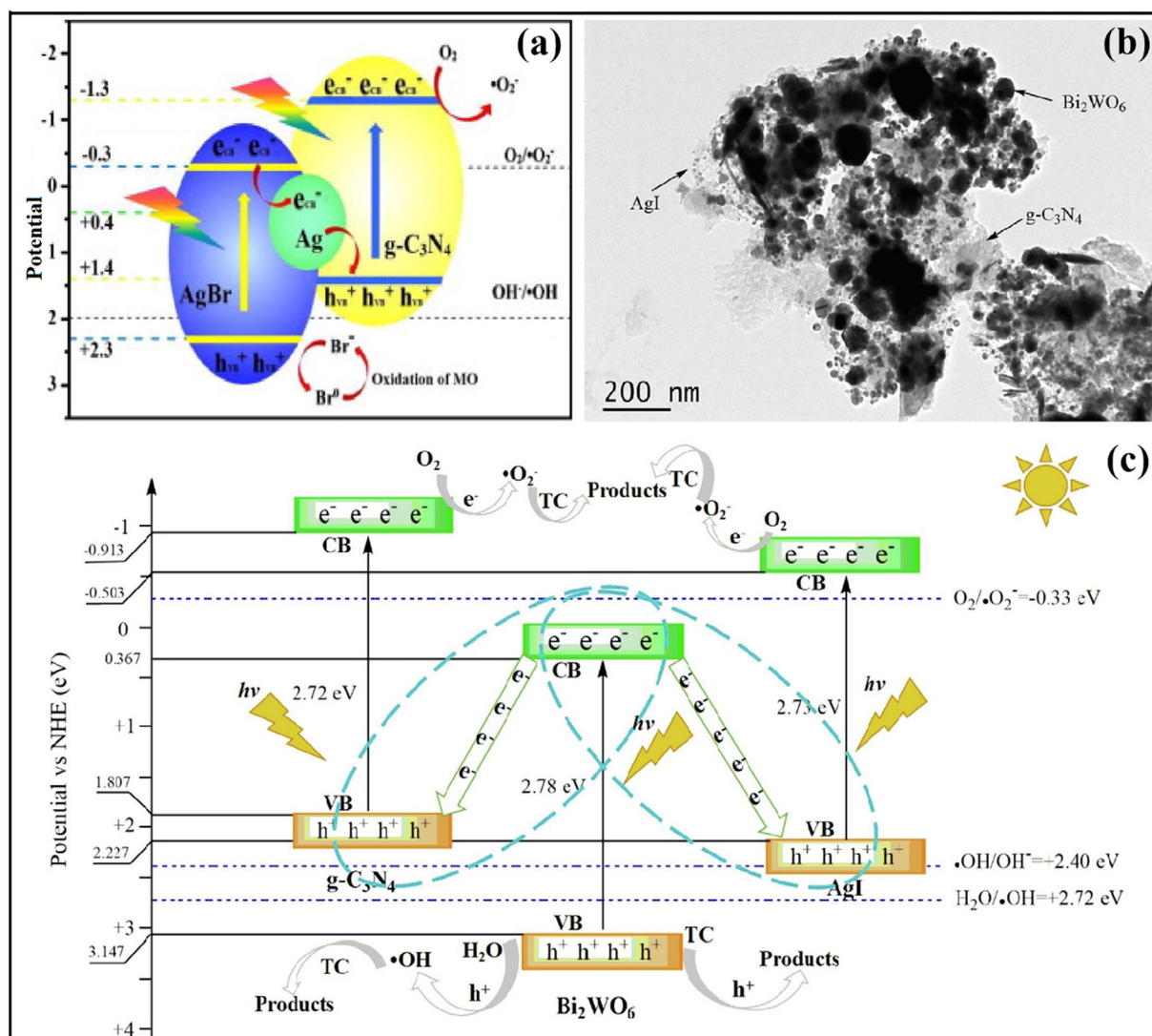


Fig. 18 (a) Mechanistic view of Ag@AgBr/g-C₃N₄ nanocomposite; reproduced with permission from Elsevier (Licence no. 4751150026281) (Yang et al., 2014), (b) TEM studies explicating uneven dispersal of AgI NPs onto g-C₃N₄ surface, and (c) Z-scheme charge transfer mechanism in g-C₃N₄/Bi₂WO₆/AgI nanohybrid; reproduced with permission from Elsevier (Licence no. 4751171004447) (Xue et al., 2019).

g-C₃N₄ (0.97 mA cm⁻²), BiVO₄ (0.03 mA cm⁻²), and Ag/AgCl/BiVO₄ (0.03 mA cm⁻²) at a potential ranging between -0.6 V and 0.5 V, as depicted in Fig. 19b. After exposure to light (150 W) the photocurrent density improved instantaneously in CAB-1 (17.5 mA cm⁻²) proceeded by g-C₃N₄-BiVO₄ (12.67 mA cm⁻²), Ag/AgCl-BiVO₄ (5.24 mA cm⁻²), g-C₃N₄ (4.25 mA cm⁻²) and BiVO₄ (0.91 mA cm⁻²). Also, the positive Mott-Schottky (MS) slopes (Fig. 19c and d) specified that both BiVO₄ and g-C₃N₄ were n-type semiconducting materials, as revealed by LSV measurements (Tachikawa et al., 2016) and retained the similar properties after the construction of flower-shaped microstructure. The PEC outcomes are in arrangement with EIS calculations. Nyquist studies (Fig. 19e) signified reduced charge transferal resistance (R_{ct}) and segregation of photo-induced charge haulers in the as-prepared microstructure. g-C₃N₄/Ag/AgCl/BiVO₄ composite follows the Z-scheme mechanism for the photocatalytic alter-

ation of CO₂ to CH₄, where Ag/AgCl act as an e⁻ sink. Both BiVO₄ and g-C₃N₄ were excited under visible light resulting in the generation of h⁺ and e⁻ in their particular E_{VB} and E_{CB}. Ag and AgCl were present in vicinity; the polarization effect of AgCl inclines to alter the charge density of Ag, followed by generation of various partial positive as well as negatively charged regions on its surface. Moreover, the Schottky barrier formed among BiVO₄ and Ag/AgCl leads to the smooth flow of e_{CB}⁻ of BiVO₄ onto Ag/AgCl surface. The h_{VB}⁺ of g-C₃N₄ transferred towards Ag/AgCl to eliminate the inward e_{CB}⁻ of BiVO₄ and to counteract the polarization effect of AgCl. This mechanistic insight helped in the dissociation of h⁺ in E_{VB} of BiVO₄ and e⁻ in E_{CB} of g-C₃N₄ to accomplish the photocatalytic reaction. The water oxidation takes place at VB of BiVO₄ to generate active protons and these protons couples through e⁻ from E_{CB} of g-C₃N₄ to reduce CO₂ into CH₄ (Rather et al., 2018).

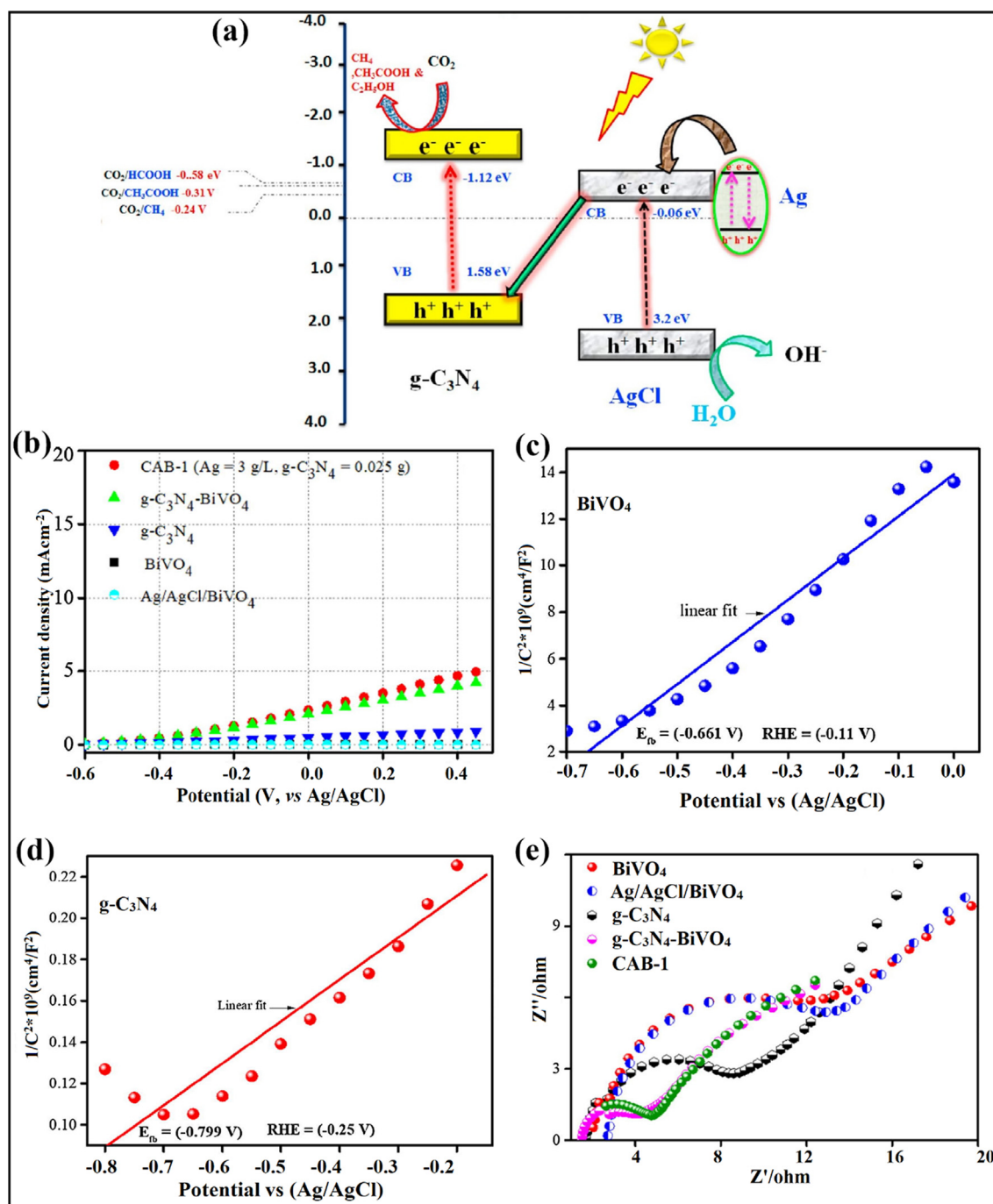


Fig. 19 (a) Schematic representation of Z-scheme charge transfer mechanism in AgCl@g-C₃N₄ nanocomposite; reproduced with permission from Elsevier (Licence no. 4751201294275) (Murugesan et al., 2018a, 2018b), photocurrent density of photocatalyst in (b) Absence of light, Mott-Schottky slopes of (c) BiVO₄, (d) g-C₃N₄, and (e) Nyquist plot of as-fabricated photocatalyst; reprinted with permission from Elsevier (Licence no. 4752980086692) (Rather et al., 2018).

4.2. Hydrogen (H₂) evolution by OWS

Li et al. tailored g-C₃N₄-Ag/AgBr (CNA) heterostructure via solvothermal technique. N₂ adsorption-desorption isotherms confirmed that g-C₃N₄ and CNA own H₃ kind of hysteric hoop, which specified that porous arrangements were initiated from an accumulation of lamellar assemblies. Also, BET surface areas of g-C₃N₄ and CNA were found to be 69.71 m²/g and 17.16 m²/g, correspondingly. The reduced

BET surface area was because of the presence of AgBr NPs, which may obstruct the pore structure of g-C₃N₄ NS for apt particle size, shown in Fig. 20a. EDX mappings were employed to explore the elemental configuration of CNA surface and confirmed the existence of C, N, Ag, and Br elements. UV-Vis DRS spectra (Fig. 20b) demonstrated that AgBr was *in-situ* deposited on the surface of g-C₃N₄ to enhance the light response. The detailed mechanism (Fig. 20c) explicated the transference of e_{CB}⁻ of g-C₃N₄ to more negative e_{CB}⁻ of AgBr,

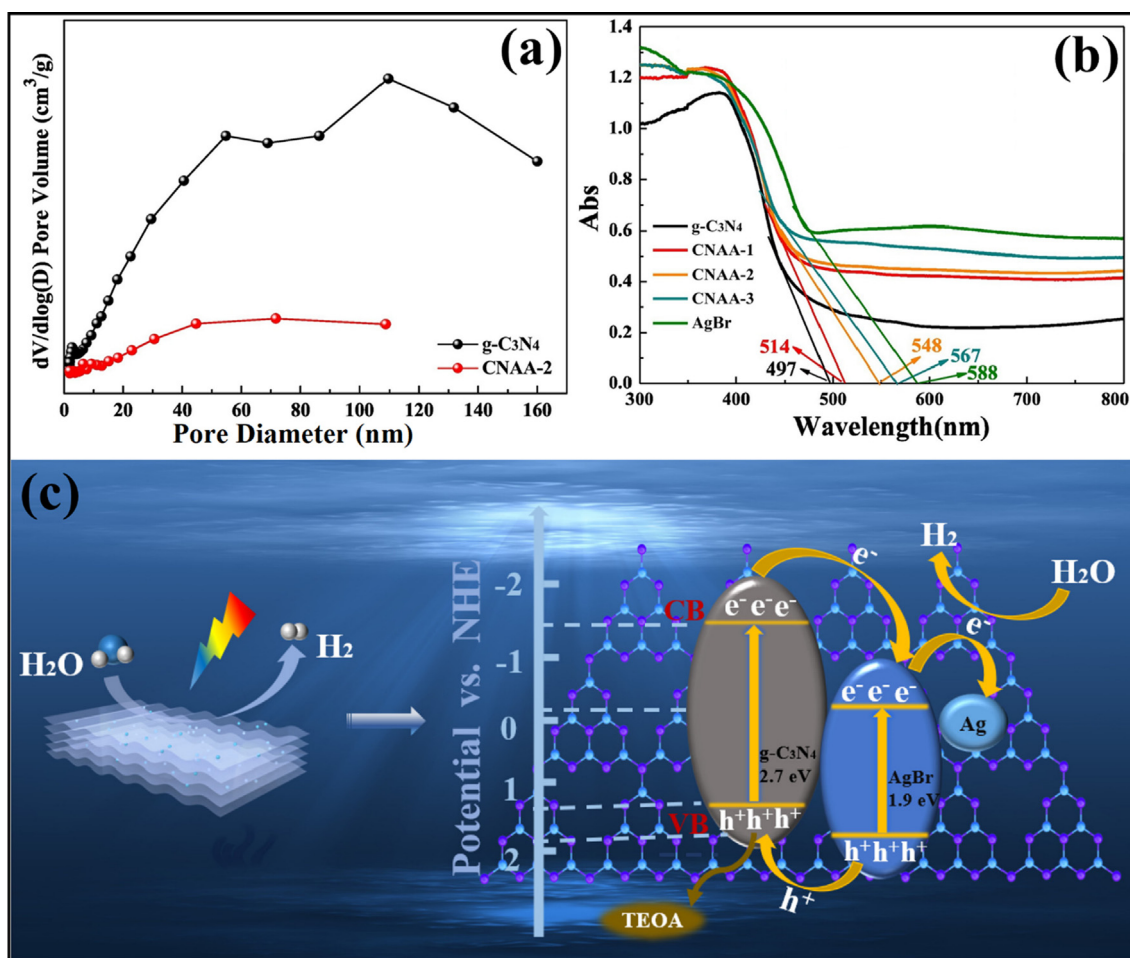


Fig. 20 (a) BET surface area of g-C₃N₄-Ag/AgBr nano-heterostructure, (b) UV-Visible spectra revealing deposition of AgBr onto g-C₃N₄ NS, and (c) Mechanistic insight of charge transfer and generation of reactive radical species in g-C₃N₄-Ag/AgBr nanohybrid; reproduced with permission from Elsevier (Licence no. 4752990867947) (Li et al., 2019).

followed by the migration of photo-excited e^- to Ag plasma. The hydrogen evolution rate (HER) ($H_2O + e^- \rightarrow H_2$) for high-density e^-_{CB} of AgBr, as well as Ag plasmas, can easily induce greater negative potential than hydrogen reduction potentials (ϕ_{H_2/H^+}). Instantaneously, h^+_{VB} of g-C₃N₄ and AgBr were straightaway apprehended and quenched by additional TEOA, thus obstructing the recombination of photo-carriers, thereby producing oxidative active radicals (Li et al., 2019). Li et al. explored construction g-C₃N₄/graphene oxide-Ag/AgBr Z-scheme composite for effective H₂ evolution (Li et al., 2019). Another work by Bai and the research group reported Ag/AgX (X = Cl, Br, I)/g-C₃N₄ nanocomposite for photocatalytic H₂ evolution (Bai et al., 2019).

4.3. Microbial inactivation

Deng et al. synthesized g-C₃N₄-AgBr composite by anchoring AgBr NPs on the g-C₃N₄ surface for photocatalytic bacterial disinfection. The antibacterial activities for Gram-negative strain *Escherichia coli* (*E. coli*) and Gram-positive strain *Staphylococcus aureus* (*S. aureus*) were analyzed under illumination of solar light. Comprehensive deactivation of 3×10^6 CFU/mL feasible cell density was fulfilled in 60 min

for *E. coli* and 150 min for *S. aureus*, correspondingly. During photocatalytic process, Ag⁺ released does not take part in disinfection activities. The photocatalytic microbial inactivation of g-C₃N₄-xAgBr (x = 0.5, 1, 2, 4) headed for *E. coli* was explored. g-C₃N₄-AgBr wholly deactivated 6.5 log *E. coli* in 60 min, whereas 1.2 log, 2.0 log, and 1.67 log reduction of feasible cell density were detected for g-C₃N₄-0.5 AgBr, g-C₃N₄-2 AgBr, and g-C₃N₄-4 AgBr within the elongated reaction time of 70 min, respectively. No considerable modification of viable cell density of Gram-positive *S. aureus* was perceived for the shady as well as blank control experimentations. The results suggested that the feasibility of *S. aureus* would be affected by either visible light emission or the direct contact with g-C₃N₄-AgBr NPs under dark surroundings. Minimal inactivation activities toward *S. aureus* were perceived for bulk g-C₃N₄ owing to its elevated rate of recombination. Comparable to *E. coli*, g-C₃N₄-AgBr photocatalyst unveiled exceptional germicidal effects to *S. aureus*. Deactivation kinetics of g-C₃N₄-AgBr for *S. aureus* was somewhat slower than that of *E. coli* (Deng et al., 2017).

Murugesan and research group investigated AgI@g-C₃N₄ photocatalyst exhibiting enhanced antimicrobial properties prepared by the deposition-precipitation approach. The

photocatalytic performance of AgI@g-C₃N₄ nanocomposite for bacterial disinfection of *E. Coli* was studied employing the disc diffusion process (Murugesan et al., 2018a, 2018b). In another work, Raizada et al. explored highly efficient photocatalyst with superior visible light activity for pollutant exclusion and bacterial disinfection (Raizada et al., 2019d).

5. Conclusion and perspectives

Over past years, photocatalysis has been established as most alluring technologies that have spurred massive attention of investigators for various environmental remediations. A photocatalyst must possess physio-chemical stability, optimum redox potential, and more excellent solar light absorption for several applications. A multifunctional metal-free g-C₃N₄ has been developed as a cost-effective photocatalytic material since 2009, owing to its chemical stability, non-toxic nature, π-conjugated, and highly porous structure, facile preparation, and improved charge transference and separation. The electronic structure endows its potential implementations as a catalyst. The e_{CB}⁻ of g-C₃N₄ possesses the superior reducing ability, which can be employed for photocatalytic water splitting, H₂ evolution, reduction of CO₂ to hydrocarbon fuels, bacterial decontamination, and pollutant mineralization. The cornucopia possessions linked with g-C₃N₄ nanomaterial have unusually improved its photocatalytic efficacy. Moreover, for bulk g-C₃N₄, it would be problematic to own high stability, effective spatial charge separation, superior absorption range, and redox ability, which bounds its practical use. To overcome these deficits, specific criteria have to be satisfied these are; (i) natural light-harvesting (complete utilization of solar energy), (ii) facilitated the separation of photo-generated charge carriers, and (iii) enhancing surface area for surface adsorption and reaction. Moreover, g-C₃N₄ can be simply prepared via thermal polymerization of a nitrogen-rich precursor. Apart, g-C₃N₄ sheets act as deposition sites for the loading of NPs to form a hybrid system. Plasmonic photocatalyst composed of noble metal NPs (Ag, Au) revealed more excellent absorption in the visible range, which may be attributable to their strong SPR effect. Also, Ag NPs were preferred over Au NPs owing to their cost effectiveness comparable to Au NPs. We have encapsulated recent progressions on Ag-based compounds due to their potential applications in catalysis, biosensing, and biomedicines. To date, ample investigations based on AgX (X = Cl, Br, I) have been explored due to its various photocatalytic applications utilizing solar light for environmental restoration and energy output. However, due to the reactive nature of fluorine, AgF has demised its applicability as photocatalyst. Plasmonic AgX possessing antibacterial properties have emerged as photosensitive material with prolonged visible light absorption. Nevertheless, AgX being wide-ranging semiconductors, they have evolved as visible-light-driven photocatalyst. Due to strong photosensitivity, AgX undergoes a reduction of Ag⁺ to Ag⁰ under exposure to visible light, thereby decreasing the stability and lifetime. AgX has wide-spread implementations in photographic films as well as used as photosensitizers and a metallic precursor for silver. However, Ag-based semiconductors were unstable and photochemically corrosive, restricting the practical applications of AgX as photocatalytic material. Also, bare AgX

NPs can easily agglomerate any may cause decreased efficiency of a photocatalyst.

The evolution of nano-junctions by hybridizing a semiconductor with another semiconducting material of almost comparable energy, as co-catalyst to form various heterostructures, has been regarded as an advanced paradigm towards boosted photocatalytic efficiency. A tremendous work emphasizing AgX/g-C₃N₄ (X = Cl, Br, I) nanoarchitectures has been reported to date. g-C₃N₄ grafted AgX heterojunctions could depress spatial charge separation, thereby boosting visible light absorption. Moreover, g-C₃N₄ tailored AgX nano-junctions can be employed for various practical implementations, for instance, overall water splitting to H₂ and O₂, CO₂ conversion to energy fuels, toxin removal, and microbial decontamination. In the focus of this review, we have divided heterostructures into two main classes, accurately type-II heterojunctions and Z-scheme heterojunction process. Several reports based on type-II and Z-scheme found AgX/g-C₃N₄ nanostructures exploring photodegradation of organic pollutants have been discussed in this review. At the same time, multifunctional applications for g-C₃N₄ anchored AgX nano-hybrids have also been analyzed.

6. Challenges and outlooks

Despite admirable results stated, the investigations in this arena are still in initial phases, and more advances are prominently necessitated as discussed underneath;

- (1) The work suffers from lower efficacy as well as inferior stability of nano-hybrid, which are distant from the necessities of industrial needs.
- (2) Advanced characterization of interfacial imageries remains a challenge for investigators. Subsequently, the decay of Ag-based compounds is often unpreventable when illuminated to a high energy e⁻ beam.
- (3) For extensive fabrication of a nano photocatalyst, an expedient and facile approach is the Holy Grail.
- (4) Theoretically, the charge transfer and separation pathway could be well understood, but more experimental pieces of evidence are necessary to support these photochemical mechanisms and provided evidences to construct an effectual photocatalytic system.
- (5) Systematic estimation of photocatalytic material in a comprehensive way should be examined, for example overall waste water splitting, organic synthesis, and conversions, which usually occur by UV excitation.
- (6) Visible light assisted photocatalyst employed for various practical applications for environmental clean-up, utilizing green energy and light-reaping devices, there is still a long way to go.
- (7) So far, several issues need to be fixed for energy to fuel cells alteration before employing at commercial scale, to increase the quantum yield and reaction efficiency
- (8) Lesser absorption of solar light is the bottleneck of a photocatalytic material inhibiting the lifetime of the photocatalyst in everyday implementations.
- (9) The photo corrosive nature of Ag-based compounds owing to the reduction of Ag⁺ to Ag⁰ is the obstruction limiting its potential applications.

Therefore, achievements and contributions in this field of exploration have aimed at a scientific community for commercial applications.

Declaration of Competing Interest

The authors declare that they have no known competing financial interests or personal relationships that could have appeared to influence the work reported in this paper.

References

- Ai, C., Wu, S., Li, L., Lei, Y., Shao, X., 2019. Novel magnetically separable γ -Fe₂O₃/Ag/AgCl/g-C₃N₄ composite for enhanced disinfection under visible light. *Colloids Surf., A* 583, 123981.
- Akbarzadeh, R., Fung, C.S., Rather, R.A., Lo, I.M., 2018. One-pot hydrothermal synthesis of g-C₃N₄/Ag/AgCl/BiVO₄ micro-flower composite for the visible light degradation of ibuprofen. *Chem. Eng. J.* 341, 248–261.
- Akhundi, A., Habibi-Yangjeh, A., 2015a. Novel magnetic g-C₃N₄/Fe₃O₄/AgCl nanocomposites: Facile and large-scale preparation and highly efficient photocatalytic activities under visible-light irradiation. *Mater. Sci. Semicond. Process.* 39, 162–171.
- Akhundi, A., Habibi-Yangjeh, A., 2015b. Novel magnetically separable g-C₃N₄/AgBr/Fe₃O₄ nanocomposites as visible-light-driven photocatalysts with highly enhanced activities. *Ceram. Int.* 41 (4), 5634–5643.
- Akhundi, A., Habibi-Yangjeh, A., 2015c. Ternary g-C₃N₄/ZnO/AgCl nanocomposites: synergistic collaboration on visible-light-driven activity in photodegradation of an organic pollutant. *Appl. Surf. Sci.* 358, 261–269.
- Akhundi, A., Habibi-Yangjeh, A., 2016a. Codeposition of AgI and Ag₂CrO₄ on g-C₃N₄/Fe₃O₄ nanocomposite: Novel magnetically separable visible-light-driven photocatalysts with enhanced activity. *Adv. Powder Technol.* 27 (6), 2496–2506.
- Akhundi, A., Habibi-Yangjeh, A., 2016b. Novel g-C₃N₄/Ag₂SO₄ nanocomposites: fast microwave-assisted preparation and enhanced photocatalytic performance towards degradation of organic pollutants under visible light. *J. Colloid Interface Sci.* 482, 165–174.
- Akhundi, A., Habibi-Yangjeh, A., 2016c. Ternary magnetic g-C₃N₄/Fe₃O₄/AgI nanocomposites: novel recyclable photocatalysts with enhanced activity in degradation of different pollutants under visible light. *Mater. Chem. Phys.* 174, 59–69.
- Appavu, B., Kannan, K., Thiripuranthagan, S., 2016. Enhanced visible light photocatalytic activities of template free mesoporous nitrogen doped reduced graphene oxide/titania composite catalysts. *J. Ind. Eng. Chem.* 36, 184–193.
- Archana, P.S., Pachauri, N., Shan, Z., Pan, S., Gupta, A., 2015. Plasmonic enhancement of photoactivity by gold nanoparticles embedded in hematite films. *J. Phys. Chem. C* 119 (27), 15506–15516.
- Asadzadeh-Khaneghah, S., Habibi-Yangjeh, A., Abedi, M., 2018. Decoration of carbon dots and AgCl over g-C₃N₄ nanosheets: novel photocatalysts with substantially improved activity under visible light. *Sep. Purif. Technol.* 199, 64–77.
- Awazu, K., Fujimaki, M., Rockstuhl, C., Tominaga, J., Murakami, H., Ohki, Y., Watanabe, T., 2008. A plasmonic photocatalyst consisting of silver nanoparticles embedded in titanium dioxide. *J. Am. Chem. Soc.* 130 (5), 1676–1680.
- Azimi, E.B., Badii, A., Sadr, M.H., 2018. Dramatic visible photocatalytic performance of g-C₃N₄-based nanocomposite due to the synergistic effect of AgBr and ZnO semiconductors. *J. Phys. Chem. Solids* 122, 174–183.
- Bai, C., Bi, J., Wu, J., Xu, Y., Wohlrab, S., Han, Y., Zhang, X., 2019. In-situ solid-phase fabrication of Ag/AgX (X = Cl, Br, I)/g-C₃N₄ composites for enhanced visible-light hydrogen evolution. *Int. J. Hydrogen Energy* 44 (39), 21397–21405.
- Banerjee, S., Pillai, S.C., Falaras, P., O'shea, K.E., Byrne, J.A., Dionysiou, D.D., 2014. New insights into the mechanism of visible light photocatalysis. *J. Phys. Chem. Lett.* 5 (15), 2543–2554.
- Bao, Y., Chen, K., 2016. AgCl/Ag/g-C₃N₄ hybrid composites: preparation, visible light-driven photocatalytic activity and mechanism. *Nano-micro Lett.* 8 (2), 182–192.
- Barzegar, J., Habibi-Yangjeh, A., Akhundi, A., Vadivel, S., 2018a. Novel ternary g-C₃N₄/Ag₃VO₄/AgBr nanocomposites with excellent visible-light-driven photocatalytic performance for environmental applications. *Solid State Sci.* 78, 133–143.
- Barzegar, J., Habibi-Yangjeh, A., Mousavi, M., 2018b. Combination of Ag₂CrO₄ and AgI semiconductors with g-C₃N₄: Novel nanocomposites with substantially improved photocatalytic performance under visible light. *Solid State Sci.* 77, 62–73.
- Bojdys, M.J., Müller, J.O., Antonietti, M., Thomas, A., 2008. Ionothermal synthesis of crystalline, condensed, graphitic carbon nitride. *Chem.–A Eur. J.* 14 (27), 8177–8182.
- Bora, L.V., Mewada, R.K., 2017. Visible/solar light active photocatalysts for organic effluent treatment: Fundamentals, mechanisms and parametric review. *Renew. Sustain. Energy Rev.* 76, 1393–1421.
- Cao, J., Zhao, Y., Lin, H., Xu, B., Chen, S., 2013. Ag/AgBr/g-C₃N₄: A highly efficient and stable composite photocatalyst for degradation of organic contaminants under visible light. *Mater. Res. Bull.* 48 (10), 3873–3880.
- Cao, S., Yu, J., 2016. Carbon-based H₂-production photocatalytic materials. *J. Photochem. Photobiol., C* 27, 72–99.
- Chandel, N., Sharma, K., Sudhaik, A., Raizada, P., Hosseini-Bandegharai, A., Thakur, V.K., Singh, P., 2020. Magnetically separable ZnO/ZnFe₂O₄ and ZnO/CoFe₂O₄ photocatalysts supported onto nitrogen doped graphene for photocatalytic degradation of toxic dyes. *Arabian J. Chem.* 13, 4324–4340.
- Chen, D., Wang, Z., Du, Y., Yang, G., Ren, T., Ding, H., 2015a. In situ ionic-liquid-assisted synthesis of plasmonic photocatalyst Ag/AgBr/g-C₃N₄ with enhanced visible-light photocatalytic activity. *Catal. Today* 258, 41–48.
- Chen, X., Dai, Y., Wang, X., 2015b. Methods and mechanism for improvement of photocatalytic activity and stability of Ag₃PO₄: a review. *J. Alloy. Compd.* 649, 910–932.
- Chen, Y., Wang, P., Liang, Y., Zhao, M., Jiang, Y., Wang, G., Wang, Y., 2019. Fabrication of a three-dimensional porous Z-scheme silver/silver bromide/graphitic carbon nitride@ nitrogen-doped graphene aerogel with enhanced visible-light photocatalytic and antibacterial activities. *J. Colloid Interface Sci.* 536, 389–398.
- Chong, M.N., Jin, B., Chow, C.W., Saint, C., 2010. Recent developments in photocatalytic water treatment technology: a review. *Water Res.* 44 (10), 2997–3027.
- Deng, J., Liang, J., Li, M., Tong, M., 2017. Enhanced visible-light-driven photocatalytic bacteria disinfection by g-C₃N₄-AgBr. *Colloids Surf., B* 152, 49–57.
- Deraz, N.M., 2018. The comparative jurisprudence of catalysts preparation methods: I. Precipitation and impregnation methods. *J. Ind Environ Chem.* 2 (1), 19–21.
- Feng, Y., Shen, J., Cai, Q., Yang, H., Shen, Q., 2015. The preparation and properties of a g-C₃N₄/AgBr nanocomposite photocatalyst based on protonation pretreatment. *New J. Chem.* 39 (2), 1132–1138.
- Fujishima, A., Honda, K., 1972. Electrochemical photolysis of water at a semiconductor electrode. *Nature* 238 (5358), 37–38.
- Fujishima, A., Rao, T.N., Tryk, D.A., 2000. Titanium dioxide photocatalysis. *J. Photochem. Photobiol., C* 1 (1), 1–21.
- Gautam, S., Shandilya, P., Priya, B., Singh, V.P., Raizada, P., Rai, R., Singh, P., 2017. Superparamagnetic MnFe₂O₄ dispersed over graphitic carbon sand composite and bentonite as magnetically recoverable photocatalyst for antibiotic mineralization. *Sep. Purif. Technol.* 172, 498–511.

- Gautam, S., Shandilya, P., Singh, V.P., Raizada, P., Singh, P., 2016. Solar photocatalytic mineralization of antibiotics using magnetically separable NiFe_2O_4 supported onto graphene sand composite and bentonite. *J. Water Process Eng.* 14, 86–100.
- Georgekutty, R., Seery, M.K., Pillai, S.C., 2008. A highly efficient Ag-ZnO photocatalyst: synthesis, properties, and mechanism. *J. Phys. Chem. C* 112 (35), 13563–13570.
- Ghosh, U., Pal, A., 2019. Graphitic carbon nitride based Z scheme photocatalysts: Design considerations, synthesis, characterization and applications. *J. Ind. Eng. Chem.* 79, 383–408.
- Grzelczak, M., Liz-Marzán, L.M., 2014. The relevance of light in the formation of colloidal metal nanoparticles. *Chem. Soc. Rev.* 43 (7), 2089–2097.
- Hasija, V., Raizada, P., Sudhaik, A., Sharma, K., Kumar, A., Singh, P., Thakur, V.K., 2019a. Recent advances in noble metal free doped graphitic carbon nitride based nanohybrids for photocatalysis of organic contaminants in water: A review. *Appl. Mater. Today* 15, 494–524.
- Hasija, V., Raizada, P., Sudhaik, A., Singh, P., Thakur, V.K., Khan, A.A.P., 2019b. Fabrication of Ag/AgI/ WO_3 heterojunction anchored P and S co-doped graphitic carbon nitride as a dual Z scheme photocatalyst for efficient dye degradation. *Solid State Sci.* 106095.
- Hasija, V., Sudhaik, A., Raizada, P., Hosseini-Bandegharai, A., Singh, P., 2019c. Carbon quantum dots supported AgI/ZnO/phosphorus doped graphitic carbon nitride as Z-scheme photocatalyst for efficient photodegradation of 2, 4-dinitrophenol. *J. Environ. Chem. Eng.* 7, (4) 103272.
- Hua, S., Qu, D., An, L., Jiang, W., Wen, Y., Wang, X., Sun, Z., 2019. Highly efficient p-type Cu_3P /n-type $\text{g-C}_3\text{N}_4$ photocatalyst through Z-scheme charge transfer route. *Appl. Catal. B* 240, 253–261.
- Huang, X., El-Sayed, I.H., Qian, W., El-Sayed, M.A., 2006. Cancer cell imaging and photothermal therapy in the near-infrared region by using gold nanorods. *J. Am. Chem. Soc.* 128 (6), 2115–2120.
- Ingram, D.B., Christopher, P., Bauer, J.L., Linic, S., 2011. Predictive model for the design of plasmonic metal/semiconductor composite photocatalysts. *ACS Catal.* 1 (10), 1441–1447.
- Islam, M.J., Reddy, D.A., Han, N.S., Choi, J., Song, J.K., Kim, T. K., 2016. An oxygen-vacancy rich 3D novel hierarchical $\text{MoS}_2/\text{BiOI}/\text{AgI}$ ternary nanocomposite: enhanced photocatalytic activity through photogenerated electron shuttling in a Z-scheme manner. *PCCP* 18 (36), 24984–24993.
- Jürgens, B., Irran, E., Senker, J., Kroll, P., Müller, H., Schnick, W., 2003. Melem (2, 5, 8-triamino-tri-s-triazine), an important intermediate during condensation of melamine rings to graphitic carbon nitride: Synthesis, structure determination by X-ray powder diffractionometry, solid-state NMR, and theoretical studies. *J. Am. Chem. Soc.* 125 (34), 10288–10300.
- Kessler, F.K., Zheng, Y., Schwarz, D., Merschjann, C., Schnick, W., Wang, X., Bojdys, M.J., 2017. Functional carbon nitride materials—design strategies for electrochemical devices. *Nat. Rev. Mater.* 2 (6), 17030.
- Kroke, E., Schwarz, M., Horath-Bordon, E., Kroll, P., Noll, B., Norman, A.D., 2002. Tri-s-triazine derivatives. Part I. From trichloro-tri-s-triazine to graphitic C_3N_4 structures. *New J. Chem.* 26 (5), 508–512.
- Kumar, A., Raizada, P., Singh, P., Saini, R., Saini, A., Hosseini-Bandegharai, A., 2019. Perspective and status of polymeric graphitic carbon nitride based Z-scheme photocatalytic systems for sustainable photocatalytic water purification. *Chem. Eng. J.* 123496.
- Lai, C., Wang, M.M., Zeng, G.M., Liu, Y.G., Huang, D.L., Zhang, C., Wu, H.P., 2016. Synthesis of surface molecular imprinted $\text{TiO}_2/\text{graphene}$ photocatalyst and its highly efficient photocatalytic degradation of target pollutant under visible light irradiation. *Appl. Surf. Sci.* 390, 368–376.
- Lan, Y., Qian, X., Zhao, C., Zhang, Z., Chen, X., Li, Z., 2013. High performance visible light driven photocatalysts silver halides and graphitic carbon nitride (X= Cl, Br, I) nanocomposites. *J. Colloid Interface Sci.* 395, 75–80.
- Lang, X., Chen, X., Zhao, J., 2014. Heterogeneous visible light photocatalysis for selective organic transformations. *Chem. Soc. Rev.* 43 (1), 473–486.
- Lei, C., Pi, M., Zhu, X., Xia, P., Guo, Y., Zhang, F., 2016. Highly efficient visible-light photocatalytic performance based on novel AgI/ $\text{g-C}_3\text{N}_4$ composite photocatalysts. *Chem. Phys. Lett.* 664, 167–172.
- Li, H., Gan, S., Wang, H., Han, D., Niu, L., 2015. Intercorrelated superhybrid of AgBr supported on graphitic- C_3N_4 -decorated nitrogen-doped graphene: high engineering photocatalytic activities for water purification and CO_2 reduction. *Adv. Mater.* 27 (43), 6906–6913.
- Li, J., Hao, H., Zhou, J., Li, W., Lei, N., Guo, L., 2017. Ag@ AgCl QDs decorated $\text{g-C}_3\text{N}_4$ nanoplates: the photoinduced charge transfer behavior under visible light and full arc irradiation. *Appl. Surf. Sci.* 422, 626–637.
- Li, W., Ma, Q., Wang, X., He, S.A., Li, M., Ren, L., 2019. Hydrogen evolution by catalyzing water splitting on two-dimensional $\text{g-C}_3\text{N}_4$ -Ag/AgBr heterostructure. *Appl. Surf. Sci.* 494, 275–284.
- Li, W., Wang, X., Li, M., He, S.A., Ma, Q., Wang, X., 2020. Construction of Z-scheme and pn heterostructure: Three-dimensional porous $\text{g-C}_3\text{N}_4/\text{graphene oxide-Ag/AgBr}$ composite for high-efficient hydrogen evolution. *Appl. Catal. B* 268, 118384.
- Liebig, J., 1844. Ueber mellon und mellonverbindungen. *Justus Liebigs Annalen der Chemie* 50 (3), 337–363.
- Liu, B., Ye, L., Wang, R., Yang, J., Zhang, Y., Guan, R., Chen, X., 2018. Phosphorus-doped graphitic carbon nitride nanotubes with amino-rich surface for efficient CO_2 capture, enhanced photocatalytic activity, and product selectivity. *ACS Appl. Mater. Interfaces* 10 (4), 4001–4009.
- Liu, J.J., Fu, X.L., Chen, S.F., Zhu, Y.F., 2011. Electronic structure and optical properties of Ag_3PO_4 photocatalyst calculated by hybrid density functional method. *Appl. Phys. Lett.* 99, (19) 191903.
- Liu, L., Qi, Y., Yang, J., Cui, W., Li, X., Zhang, Z., 2015. An AgI@ $\text{g-C}_3\text{N}_4$ hybrid core@ shell structure: stable and enhanced photocatalytic degradation. *Appl. Surf. Sci.* 358, 319–327.
- Lv, X., Wang, T., Jiang, W., 2018. Preparation of Ag@ AgCl/ $\text{g-C}_3\text{N}_4/\text{TiO}_2$ porous ceramic films with enhanced photocatalysis performance and self-cleaning effect. *Ceram. Int.* 44 (8), 9326–9337.
- Malato, S., Fernández-Ibáñez, P., Maldonado, M.I., Blanco, J., Gernjak, W., 2009. Decontamination and disinfection of water by solar photocatalysis: recent overview and trends. *Catal. Today* 147 (1), 1–59.
- Mamba, G., Mishra, A.K., 2016. Graphitic carbon nitride ($\text{g-C}_3\text{N}_4$) nanocomposites: a new and exciting generation of visible light driven photocatalysts for environmental pollution remediation. *Appl. Catal. B* 198, 347–377.
- Matheswaran, P., Thangavelu, P., Palanivel, B., 2019. Carbon dot sensitized integrative $\text{g-C}_3\text{N}_4/\text{AgCl}$ Hybrids: An synergetic interaction for enhanced visible light driven photocatalytic process. *Adv. Powder Technol.* 30 (8), 1715–1723.
- Miao, X., Ji, Z., Wu, J., Shen, X., Wang, J., Kong, L., Song, C., 2017a. $\text{g-C}_3\text{N}_4/\text{AgBr}$ nanocomposite decorated with carbon dots as a highly efficient visible-light-driven photocatalyst. *J. Colloid Interface Sci.* 502, 24–32.
- Miao, X., Shen, X., Wu, J., Ji, Z., Wang, J., Kong, L., Song, C., 2017b. Fabrication of an all solid Z-scheme photocatalyst $\text{g-C}_3\text{N}_4/\text{GO}/\text{AgBr}$ with enhanced visible light photocatalytic activity. *Appl. Catal. A* 539, 104–113.
- Miklos, D.B., Remy, C., Jekel, M., Linden, K.G., Drewes, J.E., Hübner, U., 2018. Evaluation of advanced oxidation processes for water and wastewater treatment—a critical review. *Water Res.* 139, 118–131.

- Mohamed, R.M., 2015. Synthesis and characterization of AgCl@graphitic carbon nitride hybrid materials for the photocatalytic degradation of atrazine. *Ceram. Int.* 41 (1), 1197–1204.
- Mousavi, M., Habibi-Yangjeh, A., 2017. Novel magnetically separable g-C₃N₄/Fe₃O₄/Ag₃PO₄/Co₃O₄ nanocomposites: visible-light-driven photocatalysts with highly enhanced activity. *Adv. Powder Technol.* 28 (6), 1540–1553.
- Mousavi, M., Habibi-Yangjeh, A., 2018a. Decoration of Fe₃O₄ and CoWO₄ nanoparticles over graphitic carbon nitride: novel visible-light-responsive photocatalysts with exceptional photocatalytic performances. *Mater. Res. Bull.* 105, 159–171.
- Mousavi, M., Habibi-Yangjeh, A., 2018b. Magnetically recoverable highly efficient visible-light-active g-C₃N₄/Fe₃O₄/Ag₂WO₄/AgBr nanocomposites for photocatalytic degradations of environmental pollutants. *Adv. Powder Technol.* 29 (1), 94–105.
- Murugesan, P., Narayanan, S., Manickam, M., Murugesan, P.K., Subbiah, R., 2018a. A direct Z-scheme plasmonic AgCl@ g-C₃N₄ heterojunction photocatalyst with superior visible light CO₂ reduction in aqueous medium. *Appl. Surf. Sci.* 450, 516–526.
- Murugesan, P., Narayanan, S., Matheswaran, M., 2018b. Photocatalytic performance and antibacterial activity of visible light driven silver iodide anchored on Graphitic-C₃N₄ binary composite. *Environ. Nanotechnol. Monit. Manage.* 10, 253–263.
- Ong, W.J., Tan, L.L., Ng, Y.H., Yong, S.T., Chai, S.P., 2016. Graphitic carbon nitride (g-C₃N₄)-based photocatalysts for artificial photosynthesis and environmental remediation: are we a step closer to achieving sustainability?. *Chem. Rev.* 116 (12), 7159–7329.
- Oregan, B., Grätzel, M., 1991. A low-cost, high-efficiency solar cell based on dye-sensitized colloidal TiO₂ films. *Nature* 353 (6346), 737.
- Pare, B., Singh, P., Jonnalagadda, S.B., 2009. Degradation and mineralization of victoria blue B dye in a slurry photoreactor using advanced oxidation process.
- Patial, S., Hasija, V., Raizada, P., Singh, P., Singh, A.A.P.K., Asiri, A.M., 2020. Tunable photocatalytic activity of SrTiO₃ for water splitting: Strategies and Future scenario. *J. Environ. Chem. Eng.* 103791.
- Pawar, R.C., Kang, S., Park, J.H., Kim, J.H., Ahn, S., Lee, C.S., 2017. Evaluation of a multi-dimensional hybrid photocatalyst for enrichment of H₂ evolution and elimination of dye/non-dye pollutants. *Catal. Sci. Technol.* 7 (12), 2579–2590.
- Primo, A., Marino, T., Corma, A., Molinari, R., Garcia, H., 2011. Efficient visible-light photocatalytic water splitting by minute amounts of gold supported on nanoparticulate CeO₂ obtained by a biopolymer templating method. *J. Am. Chem. Soc.* 133 (18), 6930–6933.
- Priya, B., Shandilya, P., Raizada, P., Thakur, P., Singh, N., Singh, P., 2016. Photocatalytic mineralization and degradation kinetics of ampicillin and oxytetracycline antibiotics using graphene sand composite and chitosan supported BiOCl. *J. Mol. Catal. A: Chem.* 423, 400–413.
- Raizada, P., Gautam, S., Priya, B., Singh, P., 2016. Preparation and photocatalytic activity of hydroxyapatite supported BiOCl nanocomposite for oxytetracycline removal. *Adv. Mater. Lett* 7 (4), 312–318.
- Raizada, P., Kumar, A., Singh, P., 2020. Graphitic carbon nitride-based new advanced materials for photocatalytic applications. *Curr. Anal. Chem.* 16, 1.
- Raizada, P., Kumari, J., Shandilya, P., Dhiman, R., Singh, V.P., Singh, P., 2017a. Magnetically retrievable Bi₂WO₆/Fe₃O₄ immobilized on graphene sand composite for investigation of photocatalytic mineralization of oxytetracycline and ampicillin. *Process Saf. Environ. Prot.* 106, 104–116.
- Raizada, P., Kumari, J., Shandilya, P., Singh, P., 2017b. Kinetics of photocatalytic mineralization of oxytetracycline and ampicillin using activated carbon supported ZnO/ZnWO₄. *Desalin. Water Treat.* 79, 204–213.
- Raizada, P., Shandilya, P., Singh, P., Thakur, P., 2017c. Solar light-facilitated oxytetracycline removal from the aqueous phase utilizing a H₂O₂/ZnWO₄/CaO catalytic system. *J. Taibah Univ. Sci.* 11 (5), 689–699.
- Raizada, P., Singh, P., Kumar, A., Sharma, G., Pare, B., Jonnalagadda, S.B., Thakur, P., 2014. Solar photocatalytic activity of nano-ZnO supported on activated carbon or brick grain particles: role of adsorption in dye degradation. *Appl. Catal. A* 486, 159–169.
- Raizada, P., Sudhaik, A., Singh, P., Hosseini-Bandegharai, A., Gupta, V.K., Agarwal, S., 2019a. Silver-mediated Bi₂O₃ and graphitic carbon nitride nanocomposite as all solid state Z scheme photocatalyst for imidacloprid pesticide abatement from water. *Desalin. Water Treat.* 171, 344–355.
- Raizada, P., Sudhaik, A., Singh, P., Hosseini-Bandegharai, A., Thakur, P., 2019b. Converting type II AgBr/VO into ternary Z scheme photocatalyst via coupling with phosphorus doped g-C₃N₄ for enhanced photocatalytic activity. *Sep. Purif. Technol.*, 115692
- Raizada, P., Sudhaik, A., Singh, P., Shandilya, P., Gupta, V.K., Hosseini-Bandegharai, A., Agrawal, S., 2019c. Ag₃PO₄ modified phosphorus and sulphur co-doped graphitic carbon nitride as a direct Z-scheme photocatalyst for 2, 4-dimethyl phenol degradation. *J. Photochem. Photobiol., A* 374, 22–35.
- Raizada, P., Sudhaik, A., Singh, P., Shandilya, P., Saini, A.K., Gupta, V.K., Hosseini-Bandegharai, A., 2019d. Fabrication of Ag₃VO₄ decorated phosphorus and sulphur co-doped graphitic carbon nitride as a high-dispersed photocatalyst for phenol mineralization and E. coli disinfection. *Sep. Purif. Technol.* 212, 887–900.
- Raizada, P., Sudhaik, A., Singh, P., Shandilya, P., Thakur, P., Jung, H., 2020a. Visible light assisted photodegradation of 2, 4-dinitrophenol using Ag₂CO₃ loaded phosphorus and sulphur co-doped graphitic carbon nitride nanosheets in simulated wastewater. *Arabian J. Chem.* 13, 3196–3209.
- Raizada, P., Thakur, P., Sudhaik, A., Singh, P., Thakur, V.K., Hosseini-Bandegharai, A., 2020b. Fabrication of dual Z-scheme photocatalyst via coupling of BiOBr/Ag/AgCl heterojunction with P and S co-doped g-C₃N₄ for efficient phenol degradation. *Arabian J. Chem.* 13, 4538–4552.
- Rather, R.A., Khan, M., Lo, I.M., 2018. High charge transfer response of g-C₃N₄/Ag/AgCl/BiVO₄ microstructure for the selective photocatalytic reduction of CO₂ to CH₄ under alkali activation. *J. Catal.* 366, 28–36.
- Sarina, S., Waclawik, E.R., Zhu, H., 2013. Photocatalysis on supported gold and silver nanoparticles under ultraviolet and visible light irradiation. *Green Chem.* 15 (7), 1814–1833.
- Shandilya, P., Mittal, D., Soni, M., Raizada, P., Hosseini-Bandegharai, A., Saini, A.K., Singh, P., 2018a. Fabrication of fluorine doped graphene and SmVO₄ based dispersed and adsorptive photocatalyst for abatement of phenolic compounds from water and bacterial disinfection. *J. Cleaner Prod.* 203, 386–399.
- Shandilya, P., Mittal, D., Soni, M., Raizada, P., Lim, J.H., Jeong, D. Y., Singh, P., 2018b. Islanding of EuVO₄ on high-dispersed fluorine doped few layered graphene sheets for efficient photocatalytic mineralization of phenolic compounds and bacterial disinfection. *J. Taiwan Inst. Chem. Eng.* 93, 528–542.
- Shandilya, P., Mittal, D., Sudhaik, A., Soni, M., Raizada, P., Saini, A.K., Singh, P., 2019. GdVO₄ modified fluorine doped graphene nanosheets as dispersed photocatalyst for mitigation of phenolic compounds in aqueous environment and bacterial disinfection. *Sep. Purif. Technol.* 210, 804–816.
- Shandilya, P., Sudhaik, A., Raizada, P., Hosseini-Bandegharai, A., Singh, P., Rahmani-Sani, A., Thakur, V., 2020. Synthesis of Eu³⁺-doped ZnO/Bi₂O₃ heterojunction photocatalyst on graphene oxide sheets for visible light-assisted degradation of 2, 4-dimethyl phenol and bacteria killing. *Solid State Sci.* 106164.
- Sharma, S., Dutta, V., Singh, P., Raizada, P., Rahmani-Sani, A., Hosseini-Bandegharai, A., Thakur, V.K., 2019. Carbon quantum

- dot supported semiconductor photocatalysts for efficient degradation of organic pollutants in water: A review. *J. Cleaner Prod.*
- Shi, H., He, R., Sun, L., Cao, G., Yuan, X., Xia, D., 2019. Band gap tuning of g-C₃N₄ via decoration with AgCl to expedite the photocatalytic degradation and mineralization of oxalic acid. *J. Environ. Sci.* 84, 1–12.
- Singh, P., Gautam, S., Shandilya, P., Priya, B., Singh, V.P., Raizada, P., 2017. Graphene bentonite supported ZnFe₂O₄ as superparamagnetic photocatalyst for antibiotic degradation. *Adv. Mater. Lett.* 8 (3), 229–238.
- Singh, P., Priya, B., Shandilya, P., Raizada, P., Singh, N., Pare, B., Jonnalagadda, S.B., 2019a. Photocatalytic mineralization of antibiotics using 60% WO₃/BiOCl stacked to graphene sand composite and chitosan. *Arabian J. Chem.* 12 (8), 4627–4645.
- Singh, P., Raizada, P., Kumari, S., Kumar, A., Pathania, D., Thakur, P., 2014. Solar-Fenton removal of malachite green with novel Fe⁰-activated carbon nanocomposite. *Appl. Catal. A* 476, 9–18.
- Singh, P., Raizada, P., Sudhaik, A., Shandilya, P., Thakur, P., Agarwal, S., Gupta, V.K., 2019b. Enhanced photocatalytic activity and stability of AgBr/BiOBr/graphene heterojunction for phenol degradation under visible light. *J. Saudi Chem. Soc.* 23 (5), 586–599.
- Singh, P., Shandilya, P., Raizada, P., Sudhaik, A., Rahmani-Sani, A., Hosseini-Bandegharaei, A., 2020. Review on various strategies for enhancing photocatalytic activity of graphene based nanocomposites for water purification. *Arabian J. Chem.* 13 (1), 3498–3520.
- Singh, P., Sharma, K., Hasija, V., Sharma, V., Sharma, S., Raizada, P., Thakur, V.K., 2019c. Systematic review on applicability of magnetic iron oxides-integrated photocatalysts for degradation of organic pollutants in water. *Mater. Today Chem.* 14, 100186.
- Sōmiya, S., Roy, R., 2000. Hydrothermal synthesis of fine oxide powders. *Bull. Mater. Sci.* 23 (6), 453–460.
- Sudhaik, A., Raizada, P., Shandilya, P., Jeong, D.Y., Lim, J.H., Singh, P., 2018a. Review on fabrication of graphitic carbon nitride based efficient nanocomposites for photodegradation of aqueous phase organic pollutants. *J. Ind. Eng. Chem.*
- Sudhaik, A., Raizada, P., Shandilya, P., Singh, P., 2018b. Magnetically recoverable graphitic carbon nitride and NiFe₂O₄ based magnetic photocatalyst for degradation of oxytetracycline antibiotic in simulated wastewater under solar light. *J. Environ. Chem. Eng.* 6 (4), 3874–3883.
- Sun, L., Liu, C., Li, J., Zhou, Y., Wang, H., Huo, P., Yan, Y., 2019. Fast electron transfer and enhanced visible light photocatalytic activity by using poly-*o*-phenylenediamine modified AgCl/g-C₃N₄ nanosheets. *Chin. J. Catal.* 40 (1), 80–94.
- Tachikawa, T., Ochi, T., Kobori, Y., 2016. Crystal-face-dependent charge dynamics on a BiVO₄ photocatalyst revealed by single-particle spectroelectrochemistry. *ACS Catal.* 6 (4), 2250–2256.
- Tang, G., Zhang, F., Huo, P., Zulfqarc, S., Xu, J., Yan, Y., Tang, H., 2019a. Constructing novel visible-light-driven ternary photocatalyst of AgBr nanoparticles decorated 2D/2D heterojunction of g-C₃N₄/BiOBr nanosheets with remarkably enhanced photocatalytic activity for water-treatment. *Ceram. Int.*
- Tang, H., Chang, S., Tang, G., Liang, W., 2017. AgBr and g-C₃N₄ co-modified Ag₂CO₃ photocatalyst: a novel multi-heterostructured photocatalyst with enhanced photocatalytic activity. *Appl. Surf. Sci.* 391, 440–448.
- Tang, M., Ao, Y., Wang, C., Wang, P., 2019b. Facile synthesis of dual Z-scheme g-C₃N₄/Ag₃PO₄/AgI composite photocatalysts with enhanced performance for the degradation of a typical neonicotinoid pesticide. *Environ. Appl. Catal. B*, 118395.
- Tate, E.W., 2012. Synthesis and Characterisation of Photocatalyst Silver/Silver Halide Nanocomposites
- Teter, D.M., Hemley, R.J., 1996. Low-compressibility carbon nitrides. *Science* 271 (5245), 53–55.
- Wang, J., An, C., Zhang, M., Qin, C., Ming, X., Zhang, Q., 2012. Photochemical conversion of AgCl nanocubes to hybrid AgCl–Ag nanoparticles with high activity and long-term stability towards photocatalytic degradation of organic dyes. *Can. J. Chem.* 90 (10), 858–864.
- Wang, K., Li, Q., Liu, B., Cheng, B., Ho, W., Yu, J., 2015. Sulfur-doped g-C₃N₄ with enhanced photocatalytic CO₂-reduction performance. *Appl. Catal. B* 176, 44–52.
- Xu, H., Yan, J., Xu, Y., Song, Y., Li, H., Xia, J., Wan, H., 2013a. Novel visible-light-driven AgX/graphite-like C₃N₄ (X = Br, I) hybrid materials with synergistic photocatalytic activity. *Appl. Catal. B* 129, 182–193.
- Xu, Y.S., Zhang, W.D., 2013. Ag/AgBr-grafted graphite-like carbon nitride with enhanced plasmonic photocatalytic activity under visible light. *ChemCatChem* 5 (8), 2343–2351.
- Xu, Y., Xu, H., Yan, J., Li, H., Huang, L., Xia, J., Shu, H., 2013b. A plasmonic photocatalyst of Ag/AgBr nanoparticles coupled with g-C₃N₄ with enhanced visible-light photocatalytic ability. *Colloids Surf., A* 436, 474–483.
- Xue, W., Huang, D., Li, J., Zeng, G., Deng, R., Yang, Y., Li, B., 2019. Assembly of AgI nanoparticles and ultrathin g-C₃N₄ nanosheets co-decorated Bi₂WO₆ direct dual Z-scheme photocatalyst: An efficient, sustainable and heterogeneous catalyst with enhanced photocatalytic performance. *Chem. Eng. J.* 373, 1144–1157.
- Xue, W., Huang, D., Zeng, G., Wan, J., Cheng, M., Zhang, C., Li, J., 2018. Performance and toxicity assessment of nanoscale zero valent iron particles in the remediation of contaminated soil: a review. *Chemosphere*.
- Yamasita, D., Takata, T., Hara, M., Kondo, J.N., Domen, K., 2004. Recent progress of visible-light-driven heterogeneous photocatalysts for overall water splitting. *Solid State Ionics* 172 (1–4), 591–595.
- Yang, Y., Guo, W., Guo, Y., Zhao, Y., Yuan, X., Guo, Y., 2014. Fabrication of Z-scheme plasmonic photocatalyst Ag@AgBr/g-C₃N₄ with enhanced visible-light photocatalytic activity. *J. Hazard. Mater.* 271, 150–159.
- Yao, S., Xue, S., Zhang, J., Shen, X., 2016. Characterization and mechanism analysis of AgBr mixed cuboid WO₃ rods with enhanced photocatalytic activity. *RSC Adv.* 6 (96), 93436–93444.
- Yao, X., Liu, X., Hu, X., 2014. Synthesis of the Ag/AgCl/g-C₃N₄ composite with high photocatalytic activity under visible light irradiation. *ChemCatChem* 6 (12), 3409–3418.
- Ye, L., Liu, J., Gong, C., Tian, L., Peng, T., Zan, L., 2012. *ACS Catal.* 2, 1677–1683.
- Ye, L., Su, Y., Jin, X., Xie, H., Zhang, C., 2014. Recent advances in BiOX (X = Cl, Br and I) photocatalysts: synthesis, modification, facet effects and mechanisms. *Environ. Sci. Nano* 1 (2), 90–112.
- Yi, H., Qin, L., Huang, D., Zeng, G., Lai, C., Liu, X., Liu, S., 2019. Nano-structured bismuth tungstate with controlled morphology: fabrication, modification, environmental application and mechanism insight. *Chem. Eng. J.* 358, 480–496.
- Yu, C., Wang, P., Wang, X., Chen, F., Yu, H., 2019. Silver-melamine nanowire-assisted synthesis of net-like AgCl–Ag/g-C₃N₄ for highly efficient photocatalytic degradation ability. *J. Alloy. Compd.* 806, 263–271.
- Zhang, G., Lin, L., Li, G., Zhang, Y., Savateev, A., Zafeirotas, S., Antonietti, M., 2018. Ionothermal synthesis of triazine–heptazine-based copolymers with apparent quantum yields of 60% at 420 nm for solar hydrogen production from “Sea Water”. *Angew. Chem. Int. Ed.* 57 (30), 9372–9376.
- Zhang, J., Zhu, Z., Jiang, J., Li, H., 2019. Fabrication of a novel AgI/LaFeO₃/g-C₃N₄ dual Z-scheme photocatalyst with enhanced photocatalytic performance. *Mater. Lett.* 127029.
- Zhang, L.W., Wang, Y.J., Cheng, H.Y., Yao, W.Q., Zhu, Y.F., 2009a. Synthesis of porous Bi₂WO₆ thin films as efficient visible-light-active photocatalysts. *Adv. Mater.* 21 (12), 1286–1290.
- Zhang, Q., Ge, J., Pham, T., Goebel, J., Hu, Y., Lu, Z., Yin, Y., 2009b. Reconstruction of silver nanoparticles by UV irradiation: tailored optical properties and enhanced stability. *Angew. Chem. Int. Ed.* 48 (19), 3516–3519.

- Zhang, S., Li, J., Wang, X., Huang, Y., Zeng, M., Xu, J., 2014. In situ ion exchange synthesis of strongly coupled Ag@ AgCl/g-C₃N₄ porous nanosheets as plasmonic photocatalyst for highly efficient visible-light photocatalysis. *ACS Appl. Mater. Interfaces* 6 (24), 22116–22125.
- Zhang, W., Zhou, L., Shi, J., Deng, H., 2017a. Fabrication of novel visible-light-driven AgI/g-C₃N₄ composites with enhanced visible-light photocatalytic activity for diclofenac degradation. *J. Colloid Interface Sci.* 496, 167–176.
- Zhang, X.T., Sato, O., Taguchi, M., Einaga, Y., Murakami, T., Fujishima, A., 2005. Self-cleaning particle coating with antireflection properties. *Chem. Mater.* 17 (3), 696–700.
- Zhang, X., Wang, Y., Liu, B., Sang, Y., Liu, H., 2017b. Heterostructures construction on TiO₂ nanobelts: A powerful tool for building high-performance photocatalysts. *Appl. Catal. B* 202, 620–641.
- Zhao, C., Yang, S. Y., Liu, Z. T., Fang, Y. P., 2012. AgCl Loaded Mesoporous Graphitic Carbon Nitride as Visible Light Photocatalyst. In: *Advanced Materials Research*, vol. 518. Trans Tech Publications, pp. 54–58.
- Zheng, Q., Shen, H., Shuai, D., 2017. Emerging investigators series: advances and challenges of graphitic carbon nitride as a visible-light-responsive photocatalyst for sustainable water purification. *Environ. Sci. Water Res. Technol.* 3 (6), 982–1001.
- Zhou, J., Liu, W., Cai, W., 2019. The synergistic effect of Ag/AgCl@ ZIF-8 modified g-C₃N₄ composite and peroxymonosulfate for the enhanced visible-light photocatalytic degradation of levofloxacin. *Sci. Total Environ.* 696, 133962.
- Zhou, L., Zhang, W., Chen, L., Deng, H., Wan, J., 2017. A novel ternary visible-light-driven photocatalyst AgCl/Ag₃PO₄/g-C₃N₄: synthesis, characterization, photocatalytic activity for antibiotic degradation and mechanism analysis. *Catal. Commun.* 100, 191–195.
- Zhou, T., Xu, Y., Xu, H., Wang, H., Da, Z., Huang, S., Li, H., 2014. In situ oxidation synthesis of visible-light-driven plasmonic photocatalyst Ag/AgCl/g-C₃N₄ and its activity. *Ceram. Int.* 40 (7), 9293–9301.
- Zhou, Y., Li, J., Liu, C., Huo, P., Wang, H., 2018. Construction of 3D porous g-C₃N₄/AgBr/rGO composite for excellent visible light photocatalytic activity. *Appl. Surf. Sci.* 458, 586–596.